Title: Impacts of vaccination and Severe Acute Respiratory Syndrome Coronavirus 2 variants Alpha and Delta on Coronavirus Disease 2019 transmission dynamics in the 15 most populous metropolitan statistical areas in the United States

Authors: Ye Chen[1], Yen Ting Lin[1], Ely F. Miller, Jacob Neumann, Abhishek Mallela, Richard G. Posner, William S. Hlavacek*

[1]These authors contributed equally.

Corresponding author. Email: wish@lanl.gov

Affiliations: Los Alamos National Laboratory, Los Alamos, New Mexico, USA (Y.T. Lin, W.S. Hlavacek); Northern Arizona University, Flagstaff, Arizona, USA (Y. Chen, E F. Miller, J. Neumann, R.G. Posner); University of California, Davis, California, USA (A. Mallela).

LA-UR-21-30374

Abstract

To characterize Coronavirus Disease 2019 (COVID-19) transmission dynamics in each of the 15 most populous metropolitan statistical areas (MSAs) in the United States (US) from January 2020 to September 2021, we extended a previously reported compartmental model accounting for effects of multiple distinct periods of social distancing by adding consideration of vaccination and Severe Acute Respiratory Syndrome Coronavirus 2 (SARS-CoV-2) variants Alpha (lineage B.1.1.7) and Delta (lineage B.1.617.2). For each MSA, we found region-specific parameterizations of the model using daily reports of new COVID-19 cases available from January 21, 2020 to August 24, 2021. In the process, we obtained estimates of the relative infectiousness of Alpha and Delta as well as their takeover times in each MSA. We find that 14-d ahead forecasts are reasonably accurate; these forecasts are being updated daily. Projections made on August 24, 2021 suggest that 5 of the 15 MSAs have already achieved herd immunity.

Keywords: Coronavirus Disease 2019 (COVID-19), Severe Acute Respiratory Syndrome Coronavirus 2 (SARS-CoV-2), vaccination, SARS-CoV-2 variant Alpha (lineage B.1.1.7), SARS-CoV-2 variant Delta (lineage B.1.617.2), mathematical model, Bayesian inference, epidemiological forecasting, epidemiological projection

Text

In 2020, Coronavirus Disease 2019 (COVID-19) transmission dynamics were significantly influenced by non-pharmaceutical interventions *(1–5)*. In 2021, other factors arose with significant impacts on disease transmission: vaccination *(6, 7)* and introduction of Severe Acute Respiratory Syndrome Coronavirus 2 (SARS-CoV-2) variants *(8, 9)*.

Mass vaccination in the United States (US) began on December 14, 2020 *(10)*, with demonstrable reduction of disease burden within vaccinated populations *(11)*. As the vaccination campaign progressed into March 2021, there was widespread reduction in disease incidence *(12)* and relaxation of state-mandated non-pharmaceutical interventions *(13)*.

In early 2021, SARS-CoV-2 variant Alpha (lineage B.1.1.7) spread across the US and became the dominant circulating strain *(14)*. By the end of July 2021, the Delta variant (lineage B.1.617.2) had supplanted Alpha *(15)*, concomitant with increases in new COVID-19 case detection *(12)*. Both Alpha and Delta are believed to be more transmissible than strains circulating earlier *(16–21)*. Importantly, vaccinated persons infected with Alpha and Delta can transmit disease *(22, 23)*.

In earlier work, with the aid of a compartmental model, we quantified the impact of non-pharmaceutical interventions on COVID-19 transmission dynamics *(5)*. We found that the multiple surges in disease incidence seen in 2020 *(12)* could be explained by changes in protective behaviors, which we referred to as social distancing. Here, to quantify the impacts of vaccination and SARS-CoV-2 variants Alpha and Delta on COVID-19 transmission dynamics, we extended the model of Lin et al. *(1)* by adding consideration of vaccination and variants with increased transmissibility. We then found region-specific parameterizations of the model using

vaccination and surveillance data available for the 15 most populous metropolitan statistical areas (MSAs) in the US.

The parameterized models provide estimates of the relative transmissibility of Alpha and Delta, as well as their takeover times in each MSA (i.e., the times at which the variants became dominant). Using the parameterized models, we projected what would happen under different intervention scenarios, including complete cessation of interventions on August 25, 2021. The results indicate a strictly downward trend in disease incidence for 5 of the 15 MSAs under all scenarios. Interestingly, continuing vaccination (at the rates of August 2021) is seen to have marginal impact on transmission dynamics.

In ongoing work, we are regularly updating our region-specific parameterizations as new vaccination and surveillance data become available *(24)*. With each update, we make a 14-d forecast of disease incidence. Here, using out-of-sample data, we show that recent forecasts made with the new models are reasonably accurate, with a slight bias toward overprediction.

Methods

Data

Daily reports of new confirmed COVID-19 cases were obtained from the GitHub repository maintained by The New York Times newspaper *(25)*. Daily reports of newly completed vaccinations were obtained from the Covid Act Now database *(26)*. County-level surveillance and vaccination data were aggregated as described previously *(5)* to obtain daily case and vaccination counts for each of the 15 most populous US MSAs, which are listed in the Appendix. In the case of a missing daily report, we imputed the missing information as described in the Appendix.

85 **Compartmental Model for Disease Transmission Dynamics**

86 We used the compartmental model illustrated in Figure 1 (and Appendix Figure 1) to
87 analyze data available for each MSA of interest. The model consists of ordinary differential
88 equations (ODEs) describing the dynamics of 40 populations (state variables) (Appendix
89 Equations 1–38). The state variables are each defined in Appendix Table 1. Model parameters
90 are defined in Tables 1 and 2. Key features of the model are described below, and a full
91 description of the model is provided in the Appendix.

92 To obtain the model of Figure 1, we extended the model of Lin et al. *(5)* by including 15
93 new populations and 28 new transitions. The new compartments and transitions, which are
94 highlighted in Figure 1, capture vaccination of susceptible and recovered persons and infected
95 non-quarantined persons without symptoms at a time-varying *per capita* rate $\mu(t)$. The value of
96 $\mu(t)$ is updated daily for consistency with MSA-specific daily reports of completed vaccinations
97 (Appendix Equation 37). The model also captures immune responses to vaccination yielding
98 varying degrees of protection and the consequences of breakthrough infection of vaccinated
99 persons. Vaccine protection against transmissible infection was taken to be variant-dependent.

100 We introduced a dimensionless step function, denoted $Y_\theta(t)$, that multiplies the disease-
101 transmission rate constant β to account for $m \in \{0,1,2\}$ variants (Appendix Equations 1–4, 18–
102 22, and 24). Thus, in the new model, the quantity $Y_\theta(t)\beta$ (vs. β alone) characterizes disease
103 transmissibility at time t. $Y_\theta(t)$ was initially assigned a value of 1, and the value of $Y_\theta(t)$ was
104 allowed to increase at times $\theta = (\theta_1, \theta_2)$ (Appendix Equation 38). The Alpha variant was
105 considered by introducing a step increase in $Y_\theta(t)$ from $y_0 \equiv 1$ to $y_1 > 1$ at time $t = \theta_1$ (the
106 Alpha takeover time), and the Delta variant was considered by introducing a step increase in

$Y_\theta(t)$ from y_1 to $y_2 > y_1$ at time $t = \theta_2 > \theta_1$ (the Delta takeover time). We constrained variant takeover (in the MSAs of interest) to 2021. We will refer to y_1 and y_2 as the Alpha and Delta transmissibility factors, respectively.

As in the original model of Lin et al. *(5)*, the extended model accounts for a series of $n + 1$ distinct social-distancing periods. These periods are characterized by two step functions: $P_\tau(t)$ and $\Lambda_\tau(t)$. The values of these functions change coordinately at times $\tau = (\tau_1, \ldots, \tau_n)$ (Appendix Equations 35 and 36), where τ_i is the start time of the ith social-distancing period after the initial social-distancing period. The value of $P_\tau(t)$ defines the setpoint steady-state fraction of the susceptible population practicing social distancing at time t, and the value of $\Lambda_\tau(t)$ defines a time scale for establishment of the steady state. The value of $\Lambda_\tau(t)$ is an eigenvalue equal to a sum of social-distancing rate constants *(5)*. We assume that vaccinated persons do not practice social distancing. We use the term "social distancing" to refer to behaviors that protect against infection.

Parameters

As indicated in Table 1, we used all MSA-specific case reporting data available up to the time of inference to infer MSA-specific values for parameters characterizing the start time of the local epidemic (t_0), local disease transmissibility of ancestral viral strains (β), local social-distancing dynamics (σ, λ_0, p_0, τ_i, λ_i and p_i, for $i = 1, \ldots, n$), local emergence of variants (θ_1, y_1, θ_2, y_2), the local rate of new case detection (f_D), and noise in local case detection and reporting (r). Values for other parameters were fixed prior to inference (Table 2); inferences are conditioned on these fixed parameter estimates. There are 20 fixed parameter values, 18 of which are taken to be applicable for all MSAs, plus settings for $\mu(t)$, a step function equal to the

current empirical *per capita* rate of vaccination *(26)*. We adopted the fixed parameter estimates of Lin et al. *(5)*. New fixed parameter estimates made in this study (for m_h, f_0, f_1, f_2, and k_V) are explained in the Appendix. We took $\mu(t) = \mu_i$ for times t throughout the ith day after January 21, 2020 (Appendix Equation 37), where μ_i is the fraction of the local population reported to complete vaccination over the most recent 1-d surveillance period *(26)*. In summary, for a given inference, the number of adjustable parameters was $2m + 3n + 5$, where m (=0, 1, or 2) is the number of variants under consideration and n $(= 0, 1, \ldots)$ is the number of distinct social-distancing periods being considered beyond an initial social-distancing period.

Auxiliary Measurement Model

We assumed that state variables of the compartmental model (Figure 1, Appendix Table 1) are related to the expected number of new cases reported on a given calendar date (and detected over a 1-d surveillance period) through an auxiliary measurement model (Appendix Equations 39 and 40). The measurement model has one parameter: f_D, the region-specific fraction of new cases detected. As a simplification, we considered f_D to be time-invariant. This simplification means that we assumed, for example, that case detection was neither limited nor strongly influenced by testing capacity, which has varied over time. This assumption is reasonable if, for example, case detection is mainly determined by presentation for testing and, moreover, the motivations and societal factors that influence presentation have remained roughly constant. One can also interpret f_D as the time-averaged case detection rate. The value of f_D was inferred jointly with the adjustable model parameter values and the value of the likelihood parameter r (see below).

Statistical Model for Noise in Case Detection and Reporting

We assumed that noise in new case detection and reporting on the ith day after January 21, 2020 is captured by a negative binomial distribution $\mathrm{NB}(r, q_i)$ centered on $I(t_i, t_{i+1})$, the expected number of new cases detected as given by the compartmental model and the auxiliary measurement model (Appendix Equations 1–40). These and other assumptions led to the likelihood function used in inference (Appendix Equations 41–43). We took the probability parameter q_i in $\mathrm{NB}(r, q_i)$ to be given by Appendix Equation 43 and the dispersion parameter r to be an adjustable parameter applicable for all days of case reporting. The value of r was inferred jointly with the adjustable model parameter values and the value of the measurement model parameter f_D.

Computational Methods

We determined the intervals of the step functions $Y_\theta(t)$, $P_\tau(t)$, and $\Lambda_\tau(t)$ (i.e., θ and τ) using the model-selection method described previously *(5)* and in the Appendix. Simulations and daily Bayesian inferences were performed as previously described *(5)* and in the Appendix. Forecast accuracy was assessed using out-of-sample data as described previously *(5)* and in the Appendix.

Results

We previously established that accurate forecasts of new COVID-19 case detection can be made for the 15 most populous MSAs in the US on the basis of region-specific parameterizations of a compartmental model that accounts for time-varying nonpharmaceutical interventions *(5)*. However, in 2021, the model lost its ability to capture disease transmission dynamics, presumably because of the impacts of vaccination and the emergence of more transmissible SARS-CoV-2 variants, namely, Alpha and Delta. To remedy this problem, we

accounted for these factors in an extension of the model of Lin et al. *(5)* (Figure 1). Details about the model extension are provided in the Appendix.

As illustrated in Figure 2, the new model is able to explain historical surveillance data (Figure 2A) and accurately forecast new imminent trends in disease incidence (Figure 2B). Results for all 15 MSAs of interest are shown in Appendix Figure 2. As can be seen in Figure 2A, surveillance data—daily reports of newly detected COVID-19 cases—available from January 21, 2020 to August 24, 2021 for the New York City MSA largely lie within the 95% credible interval of the posterior predictive distribution for new case detection, which indicates that the model has explanatory power. As can be seen in Figure 2B, on August 24, 2021, the model predicted that a peak in disease incidence would soon occur, which did occur approximately 1 week later. If the conditions of August 24, 2021 do not change, a mostly downward trend in disease incidence is expected with an end of community transmission by 2022 (Figure 2C).

The model provides insight into the impacts of social-distancing behaviors and the emergence of the Alpha and Delta variants. As can be seen in Figure 2C, the New York City MSA has experienced four surges in disease incidence. According to the model, the first surge ended because of adoption of social-distancing behaviors (to the greatest extent seen during the local epidemic), the second and third surges occurred because of relaxation of social-distancing behaviors, and the fourth surge was caused by the emergence of Delta (cf. Figure 2C and 2D). In contrast, the emergence of Alpha had little impact on disease incidence. Interestingly, vaccination contributed significantly to ending the third surge, overcoming the effects of a drop in adherence to social-distancing behaviors. Results comparable to Figures 2C and 2D are shown for all 15 MSAs of interest in Appendix Figures 3 and 4.

To quantify forecast accuracy, we compared 1-, 4-, 7-, and 14-d ahead prediction quantiles (obtained from the posterior predictive distributions for the number of new cases detected) against corresponding out-of-sample data (Figure 3). In this analysis, we considered the daily predictions made for each of the 15 MSAs of interest from July 15, 2021 to August 24, 2021 and corresponding reports of new cases, which were not used in inference. If predictions are unbiased, we would expect to see empirical coverage (the fraction of reported case numbers below the prediction quantile) match the prediction quantile, i.e., falling along the diagonal broken line in Figure 3. As can be seen, overall, there is a bias toward overprediction; however, the bias is not significant. On the basis of Figure 3, we can expect future forecasts to be reasonably accurate for up to 14 d.

Our inferences provide quantitative insights into the increased transmissibility of Alpha and Delta (y_1 and y_2) and their takeover times (θ_1 and θ_2) in each of the 15 MSAs of interest. Figure 4 shows y_1, y_2, θ_1, and θ_2 marginal posteriors obtained for the New York City MSA using surveillance data available from January 21, 2020 to August 24, 2021. Marginal posteriors for all 15 MSAs of interest are shown in Appendix Figure 5. Maximum *a posteriori* (MAP) estimates of y_1, y_2, θ_1, and θ_2 for the New York City MSA are given in Table 1 (along with MAP estimates for other jointly inferred parameters). Figure 5 provides a statistical summary of our MSA-specific MAP estimates of y_1, y_2, θ_1, and θ_2. As shown, the means of our MAP estimates for y_1 and y_2 for all 15 MSAs are 1.2 and 2.1 (Figure 5A), indicating that Alpha is approximately 20% more transmissible than pre-existing viral strains and that Delta, in turn, is approximately 75% more transmissible than Alpha. The means of our MAP estimates for θ_1 and θ_2 for all 15 MSAs, the Alpha and Delta takeover times, correspond to May 2, 2021 and June 23, 2021 (Figure 5B).

To assess the importance of continued vaccination and social distancing, we made projections for four scenarios based on region-specific parameterizations obtained using surveillance data available from January 21, 2020 to August 24, 2021 (Figure 6, Appendix Figure 6). In the first scenario, we assumed that the daily rate of vaccination for a given MSA is maintained at the average rate of vaccination achieved over the period starting on August 4, 2021 and ending on August 24, 2021. We also assumed no change in social distancing. In the second scenario, we assumed that vaccination ends but social distancing is maintained. In the third scenario, we assumed that vaccination continues (as in the first scenario) but social distancing ends. In the fourth scenario, we considered both vaccination and social distancing to end. Results for the New York City and San Francisco MSAs are shown in Figures 6A and 6B, respectively. As can be seen, in both of these MSAs, continued vaccination is predicted to have almost no impact on future disease incidence, and much less of an impact than continued social distancing. Moreover, these results indicate that the current Delta-driven surge in New York City will soon peak and then steadily decline, whereas the Delta-driven surge in San Francisco is already declining. Moreover, for San Francisco, declining disease incidence is predicted under all four scenarios considered. Projections for all 15 MSAs of interest are shown in Appendix Figure 6. Projections for four other MSAs (Los Angeles, Houston, Miami, Seattle) are similar to those for San Francisco.

On the basis of our region-specific parameterizations, we can estimate the immune and susceptible fractions of each MSA population, as well as the fractions that have achieved immunity through infection and vaccination. This information, which is important for assessing progress toward herd immunity, is shown in Figure 7 as a function of time for the New York City MSA. As can be seen, as of August 24, 2021, only 17% of the population remains

susceptible to productive infection, and a significant fraction of the susceptible population (33%) has been vaccinated. 28% of the population has been infected but not vaccinated. Results for all 15 MSAs of interest are shown in Appendix Figure 7.

Discussion

We have demonstrated that reasonably accurate daily 14-d ahead forecasts of infectious disease incidence for multiple regions can be made with Bayesian uncertainty quantification (UQ) in a data-driven, model-based, online-learning fashion in the face of changing nonpharmaceutical interventions, a mass vaccination campaign, and emergence of more infectious pathogen variants (Figures 2 and 3, Appendix Figures 2–4). We continue to make daily forecasts of new COVID-19 case detection for the 15 most populous US metropolitan areas *(24)*. In our experience, the keys to forecast accuracy with Bayesian UQ are a reliable surveillance data stream, an explanatory model for disease transmission dynamics capable of capturing relevant knowledge external to the surveillance data stream, efficient MCMC sampling, and access to adequate computational resources (i.e., computer clusters).

Our forecasting inferences provided insight into the emergence of SARS-CoV-2 variants Alpha (lineage B.1.1.7) and Delta (lineage B.1.617.2) (e.g., see Figure 4). Estimates of the increased transmissibility of Alpha and Delta (i.e., marginal posteriors for the transmissibility factors y_1 and y_2) were fairly consistent across the 15 MSAs of interest (Appendix Figure 5). By taking an average of the maximum *a posteriori* (MAP) estimates of y_1 and y_2 obtained for the 15 MSAs using surveillance data available up to August 24, 2021, we arrived at the following spatially-averaged point estimates: Alpha is 1.2 times and Delta is 2.1 times more infectious than viral strains circulating before the emergence of Alpha (Figure 5A). These estimates are

264 consistent with estimates provided in other studies *(16–21)*. Similarly, we estimated that Alpha
265 became dominant around May 2, 2021 and that Delta became dominant shortly thereafter,
266 around June 23, 2021 (Figure 5B). These estimates are consistent with viral genomics survey
267 results *(15, 27)*.

268 Using region-specific parameterizations of our compartmental model, we made 300-d
269 ahead projections to assess the impacts of nonpharmaceutical interventions and vaccination on
270 disease transmission (Figure 6, Appendix Figure 6). We considered four scenarios: maintenance
271 of the *status quo*, halting of social distancing with maintenance of vaccination, halting of
272 vaccination with maintenance of social distancing, and halting of both interventions. We found
273 that halting vaccination had a negligible impact on disease transmission, which follows from
274 assuming that the low rates of vaccination seen in August 2021 will continue. Halting social
275 distancing had a greater impact than halting vaccination. Interestingly, a strictly downward trend
276 in disease incidence was seen for 5 of the 15 MSAs considered in our projections (Appendix
277 Figure 6). These results suggest that the Los Angeles, Miami, San Francisco, Riverside, and
278 Seattle MSAs have already achieved herd immunity.

279 Currently, there is interest in whether the US (or any region) has the possibility of
280 achieving herd immunity. Assessing progress toward herd immunity for a given population
281 depends on estimates of two quantities: the population-specific basic reproduction number R_0,
282 which is related to the herd immunity threshold, and the immune fraction of the population. The
283 region-specific parameterizations of our compartmental model provide insight into the immune
284 fraction in each of the 15 MSAs of interest (Figure 7, Appendix Figure 7), as well as insights into
285 other subpopulations, such as the fraction of persons who have recovered from SARS-CoV-2
286 infection. These results complement serological survey results *(28–31)*.

We caution the reader that our study has numerous limitations. Forecasts will lose accuracy if, for example, a new SARS-CoV-2 variant with distinct features emerges. Furthermore, although forecast accuracy can be assessed readily using out-of-sample data (Figure 3), the reliability of inferred parameter values (Figure 5), projections (Figure 6), and inferences of unobserved population levels (Figure 7) is more difficult to verify. These quantities depend on an array of simplifying modeling assumptions, which are explained in the Appendix, and also on the quality of MCMC sampling. Finally, we caution that forecasting with Bayesian UQ is technically challenging, especially in an online learning context with a short turnaround time (e.g., 1 d). In our opinion, there is an urgent need for computational resources to make this approach more accessible. Development of such resources would be beneficial because Bayesian UQ is helpful in making decisions when available training data are scarce and noisy and the stakes are high.

Acknowledgments

Y.T.L. was supported by the LDRD program at Los Alamos National Laboratory. Y.C., W.S.H., E.F.M., J.N. and R.G.P. were supported by a grant from the National Institute of General Medical Sciences of the National Institutes of Health (R01GM111510). A.M. was supported by the 2020 Mathematical Sciences Graduate Internship program, which is sponsored by the Division of Mathematical Sciences of the National Science Foundation. Computational resources used in this study included Northern Arizona University's Monsoon computer cluster, which is funded by Arizona's Technology and Research Initiative Fund. Y.C. thanks Song Chen (University of Wisconsin, La Crosse, Wisconsin, USA) for technical assistance.

Author Bio

Dr. Chen is an Assistant Professor in the Department of Mathematics and Statistics at Northern Arizona University. Her research interests include high-dimensional data analysis in bioinformatics and systems biology.

References (50 maximum)

1. Courtemanche C, Garuccio J, Le A, Pinkston J, Yelowitz A.Strong social distancing measures in the United States reduced the COVID-19 growth rate. Health Aff (Millwood). 2020;39:1237–46. https://doi.org/10.1377/hlthaff.2020.00608
2. Hsiang S, Allen D, Annan-Phan S, Bell K, Bolliger I, Chong T, et al. The effect of large-scale anti-contagion policies on the COVID-19 pandemic. Nature. 2020;584:262–7. https://doi.org/10.1038/s41586-020-2404-8
3. Matrajt L, Leung T. Evaluating the effectiveness of social distancing interventions to delay or flatten the epidemic curve of coronavirus disease. Emerg Inf Dis. 2020;26:1740–8. https://doi.org/10.3201/eid2608.201093
4. Bo Y, Guo C, Lin C, Zheng Y, Li HB, et al. Effectiveness of non-pharmaceutical interventions on COVID-19 transmission in 190 countries from 23 January to 13 April 2020. Int J Inf Dis. 2021;102:247–53. https://doi.org/10.1016/j.ijid.2020.10.066
5. Lin YT, Neumann J, Miller EF, Posner RG, Mallela A, Safta C, Ray J, Thakur G, Chinthavali S, Hlavacek WS. Daily forecasting of regional epidemics of Coronavirus Disease with Bayesian uncertainty quantification, United States. Emerg Inf Dis. 2021;27:767–78. https://doi.org/10.3201/eid2703.203364

330 6. Oliver SE, Gargano JW, Marin M, Wallace M, Curran KG, Chamberland M, et al. The
331 Advisory Committee on Immunization Practices' interim recommendation for use of
332 Pfizer-BioNTech COVID-19 vaccine—United States, December 2020. MMWR Morb
333 Mortal Wkly Rep. 2020;69:1922–4. https://doi.org/10.15585/mmwr.mm6950e2
334 7. Oliver SE, Gargano JW, Marin M, Wallace M, Curran KG, Chamberland M, et al. The
335 Advisory Committee on Immunization Practices' interim recommendation for use of
336 Moderna COVID-19 vaccine—United States, December 2020. MMWR Morb Mortal
337 Wkly Rep. 2020;69:1653–6. https://doi.org/10.15585/mmwr.mm695152e1
338 8. Galloway SE, Paul P, MacCannell DR, Johansson MA, Brooks JT, MacNeil A, et al.
339 Emergence of SARS-CoV-2 B.1.1.7 lineage—United States, December 29, 2020–
340 January 12, 2021. http://dx.doi.org/10.15585/mmwr.mm7003e2
341 9. Herlihy R, Bamberg W, Burakoff A, Alden N, Severson R, Bush E, et al. Rapid increase
342 in circulation of the SARS-CoV-2 B.1.617.2 (Delta) variant—Mesa County, Colorado,
343 April–June 2021. MMWR Morb Mortal Wkly Rep. 2021;70:1084–7.
344 https://doi.org/10.15585/mmwr.mm7032e2
345 10. Department of Health and Human Services. COVID-19 vaccine distribution: the process.
346 2021 [cited 2021 Oct 6] https://www.hhs.gov/coronavirus/covid-19-
347 vaccines/distribution/index.html
348 11. Daniel W, Nivet M, Warner J, Podolsky DK. Early evidence of the effect of SARS-CoV-
349 2 vaccine at one medical center. N Engl J Med. 2021;384:1962–3.
350 https://doi.org/10.1056/NEJMc2102153
351 12. Centers for Disease Control and Prevention. COVID data tracker. 2021 [cited 2021 Oct
352 6] https://covid.cdc.gov/covid-data-tracker/#datatracker-home

13. Coronavirus Resource Center, Johns Hopkins University. Impact of opening and closing decisions by state: a look at how social distancing measures may have influenced trends in COVID-19 cases and deaths. 2021 [cited 2021 Oct 6] https://coronavirus.jhu.edu/data/state-timeline
14. Washington NL, Gangavarapu K, Zeller M, Bolze A, Cirulli ET, Schiabor Barrett KM, et al. Emergence and rapid transmission of SARS-CoV-2 B.1.1.7 in the United States. Cell. 2021;184:2587–94. https://doi.org/10.1016/j.cell.2021.03.052
15. Centers for Disease Control and Prevention. Covid data tracker, variant proportions. 2021 [cited 2021 Oct 6] https://covid.cdc.gov/covid-data-tracker/#variant-proportions
16. Volz E, Mishra S, Chand M, Barrett JC, Johnson R, Geidelberg L, et al. Assessing transmissibility of SARS-CoV-2 lineage B.1.1.7 in England. Nature. 2021;593:266–9. https://doi.org/10.1038/s41586-021-03470-x
17. Davies NG, Abbott S, Barnard RC, Jarvis CI, Kucharski AJ, Munday JD, et al. Estimated transmissibility and impact of SARS-CoV-2 lineage B.1.1.7 in England. Science. 2021;372:eabg3055. https://doi.org/10.1126/science.abg3055
18. Ito K, Piantham C, Nishiura H. Predicted dominance of variant Delta of SARS-CoV-2 before Tokyo Olympic Games, Japan, July 2021. Euro Surveill. 2021;26:2100570. https://doi.org/10.2807/1560-7917.ES.2021.26.27.2100570
19. Arav Y, Fattal E, Klausner Z. Increased transmissibility of emerging SARS-CoV-2 variants is driven either by viral load or probability of infection rather than environmental stability. https://www.medrxiv.org/content/10.1101/2021.07.19.21260707v1
20. Public Health England. SARS-CoV-2 variants of concern and variants under investigation in England. Technical briefing 15, June 11, 2021. [cited 2021 Aug 24]

376 https://assets.publishing.service.gov.uk/government/uploads/system/uploads/attachment_
377 data/file/993879/Variants_of_Concern_VOC_Technical_Briefing_15.pdf
378 21. Cascella M, Rajnik M, Aleem A, Dulebohn SC, Di Napoli R. Features, evaluation, and
379 treatment of coronavirus (COVID-19). July 30, 2021 update. Treasure Island (FL):
380 StatPearls Publishing; 2021. https://www.ncbi.nlm.nih.gov/books/NBK554776/
381 22. Lopez Bernal J, Andrews N, Gower C, Gallagher E, Simmons R, Thelwall S, et al.
382 Effectiveness of Covid-19 Vaccines against the B.1.617.2 (Delta) variant. N Engl J Med.
383 2021;385:585–94. https://doi.org/10.1056/NEJMoa2108891
384 23. Rovida F, Cassaniti I, Paolucci S, Percivalle E, Sarasini A, Piralla A, et al. SARS-CoV-2
385 vaccine breakthrough infections with the alpha variant are asymptomatic or mildly
386 symptomatic among health care workers. Nat Commun. 2021;12:6032.
387 https://doi.org/10.1038/s41467-021-26154-6
388 24. Chen Y, Lin YT, Miller EF, Neumann J, Mallela A, Chen S, Posner RG, Hlavacek WS.
389 COVID-19 Predictions [cited 2021 Oct 8] https://github.lanl.gov/lanl/covid-19-
390 predictions
391 25. The New York Times. Coronavirus (Covid-19) data in the United States. 2021 [cited
392 2021 Aug 24] https://github.com/nytimes/covid-19-data
393 26. Covid Act Now. US COVID risk and vaccine tracker. 2021 [cited 2021 Sep 29]
394 https://covidactnow.org/
395 27. Helix. The Helix COVID-19 surveillance dashboard. [cited 2021 Oct 11]
396 https://www.helix.com/pages/helix-covid-19-surveillance-dashboard/

397 28. Centers for Disease Control and Prevention. Large-scale geographic seroprevalence
398 surveys. 2021 [cited 2021 Aug 24] https://www.cdc.gov/coronavirus/2019-ncov/cases-
399 updates/geographic-seroprevalence-surveys.html
400 29. Jones JM, Stone M, Sulaeman H, Fink RV, Dave H, Levy ME, et al. Estimated US
401 infection- and vaccine-induced SARS-CoV-2 seroprevalence based on blood donations,
402 July 2020–May 2021. JAMA. 2021;e2115161 https://doi.org/10.1001/jama.2021.15161
403 30. Moghadas SM, Sah P, Shoukat A, Meyers LA, Galvani AP. Population immunity against
404 COVID-19 in the United States. Ann Intern Med. 2021;M21-2721.
405 https://doi.org/10.7326/M21-2721
406 31. O'Driscoll M, Ribeiro Dos Santos G, Wang L, Cummings DAT, Azman AS, Paireau J, et
407 al. Age-specific mortality and immunity patterns of SARS-CoV-2. Nature.
408 2021;590:140–145. https://doi.org/10.1038/s41586-020-2918-0

409

410 Address for correspondence: William S. Hlavacek, Theoretical Biology and Biophysics
411 Group, Theoretical Division, Los Alamos National Laboratory, Los Alamos, NM 87545,
412 USA; email: wish@lanl.gov

413

414

415 **Table 1.** Model parameter values inferred for the New York City Metropolitan Statistical Area

416 (MSA) on August 24, 2021

Parameter	MAP estimate* (Units)	Description
t_0	8.8 (d)	Start of local disease transmission
β	0.37 (d^{-1})	Rate constant for disease transmission
σ	67 (d)	Start of first social-distancing period
p_0	0.47	Social-distancing setpoint for the period $t \in [\sigma, \tau_1)$
λ_0	2.6 (d^{-1})	Social-distancing eigenvalue paired with p_0
τ_1	147 (d)	Start of second social-distancing period
p_1	0.39	Social-distancing setpoint for the period $t \in [\tau_1, \tau_2)$
λ_1	2.2 (d^{-1})	Social-distancing eigenvalue paired with p_1
τ_2	209 (d)	Start of third social-distancing period
p_2	0.41	Social-distancing setpoint for the period $t \in [\tau_2, \tau_3)$
λ_2	1.8 (d^{-1})	Social-distancing eigenvalue paired with p_2
τ_3	283 (d)	Start of fourth social-distancing period
p_3	0.27	Social-distancing setpoint for the period $t \in [\tau_3, \tau_4)$
λ_3	2.9 (d^{-1})	Social-distancing eigenvalue paired with p_3
τ_4	390 (d)	Start of fifth social-distancing period
p_4	0.09	Social-distancing setpoint for the period $t \in [\tau_4, \infty)$
λ_4	6.4 (d^{-1})	Social-distancing eigenvalue paired with p_4

θ_1	487 (d)	Alpha takeover time
y_1	1.4	Increased infectiousness of Alpha (relative to ancestral strains)
θ_2	14 (d)	Delta takeover time
y_2	2.3	Increased infectiousness of Delta (relative to ancestral strains)
f_D	0.33	Fraction of cases detected and reported
r	1.5	Dispersion parameter of $\mathrm{NB}(r, q_i)$**

*Maximum *a posteriori* (MAP) estimates are region-specific and inference-time-dependent. Here, inference was based on New York City MSA-specific confirmed coronavirus disease case count data available in the GitHub repository maintained by The New York Times newspaper *(25)* for January 21, 2020–August 24, 2021. Time $t = 0$ corresponds to midnight on January 21, 2020. Inferences were conditioned on the compartmental model of Appendix Equations 1–38, consideration of two viral variants (Alpha and Delta), $n = 4$ (i.e., consideration of an initial social-distancing period followed sequentially by four distinct social-distancing periods), the fixed parameter estimates of Table 2, and the initial condition defined by the estimate for t_0 and the values of I_0 and S_0 given in Table 2. The choice of two variants and the setting for n were chosen through a model-selection procedure described in the Appendix. With $m = 2$ and $n = 4$, there are 21 adjustable model parameters: t_0, β, θ_1, y_1, θ_2, y_2, σ, p_0, λ_0, τ_1, p_1, λ_1, τ_2, p_2, λ_2, τ_3, p_3, λ_3, τ_4, p_4, and λ_4. These parameters were jointly inferred together with f_D, the parameter of the measurement model (i.e., the fraction of new cases detected and reported) (Appendix Equation 40), and r, the dispersion parameter of the statistical model for noise in case detection

and reporting (i.e., the adjustable parameter of the negative binomial likelihood function) (Appendix Equations 41–43). We assumed a uniform proper prior, as described in the Appendix. **The probability parameter of $\mathrm{NB}(r, q_i)$ is constrained, i.e., the value of q_i, which is reporting time-dependent, is given by Appendix Equation 43.

436

437 **Table 2.** Fixed parameter estimates for each region-specific compartmental model

Parameter	Estimate[1] (Units)	Description	Source
I_0	1	Number of infectious persons at time $t = t_0$	*(5)*
S_0	19,216,182[2]	Total population	*(5)*
$\mu(t)$	Empirical time-series[3] (d^{-1})	Daily *per capita* rate of vaccination	*(26)*
m_b	0.1	Reduction in risk of infection because of social distancing	*(5)*
m_h	0.04	Reduction in risk of severe disease (once symptomatic) because of vaccination	This study[4]
f_A	0.44	Fraction of all cases that are asymptomatic	*(5)*
f_H	0.054	Fraction of symptomatic cases that are severe (in the absence of vaccination)	*(5)*
f_R	0.79	Fraction of persons with severe disease who recover	*(5)*
$1 - f_0$	0.1	Fraction of vaccinated persons who fail to develop an immune response that protects against productive infection by ancestral strains or variants	This study[4]

$f_0 - f_1$	0.09	Fraction of vaccinated persons who develop an immune response that protects against productive infection by ancestral strains (but not the Alpha or Delta variant)	This study[4]
$f_1 - f_2$	0.12	Fraction of vaccinated persons who develop an immune response that protects against productive infection by ancestral strains and the Alpha variant (but not the Delta variant)	This study[4]
f_2	0.69	Fraction of vaccinated persons who develop an immune response that protects against productive infection by ancestral strains and the Alpha and Delta variants	This study[4]
ρ_E	1.1	Relative infectiousness of persons without symptoms in the incubation period of infection	*(5)*
ρ_A	0.9	Relative infectiousness of persons without symptoms in the immune-clearance phase of infection	*(5)*
k_L	0.94 (d^{-1})	Rate constant for progression through each stage of the incubation period of infection[5]	*(5)*
k_Q	0.0038 (d^{-1})	Rate constant for quarantine of infected, non-vaccinated persons	*(5)*

j_Q	0.4 (d^{-1})	Rate constant for self-isolation of symptomatic, non-vaccinated persons	*(5)*
c_A	0.26 (d^{-1})	Rate constant for completion of the immune clearance phase of infection for persons without symptoms	*(5)*
c_I	0.12 (d^{-1})	Rate constant for completion of the immune clearance phase of infection or progression to severe disease for non-vaccinated persons with symptoms	*(5)*
c_H	0.17 (d^{-1})	Rate constant for recovery or progression to death for non-vaccinated persons with severe disease	*(5)*
k_V	0.3 (d^{-1})	Rate constant for progression through each stage of immune response to vaccination[6]	This study[4]

[1]Fixed parameter estimates are based on information external to the surveillance data used to infer the adjustable parameter values of Table 1. Estimates are applicable to all metropolitan statistical areas (MSAs) of interest except for S_0 and the time-series $\mu(t)$, which are region-specific.

[2]The total population S_0 is MSA-specific. Here, S_0 is given for the New York City MSA. The initial susceptible population is taken to be the total population.

[3]The time-series $\mu(t)$ is determined by region-specific vaccination data *(26)*: $\mu(t) = \mu_i$ for $t \in [t_i, t_{i+1})$, where t_i is midnight on the ith day after January 21, 2020. The quantity μ_i was chosen

so that $\mu_i S_0 \times 1$ d corresponds to the number of vaccinations completed over the past 1-d period closest to the ith day after January 21, 2020.

[4]See the Appendix for estimates of fixed parameter values made in this study.

[5]As in the study of Lin et al. *(5)*, the incubation period is divided into 5 stages (Figure 1), each of equal duration on average.

[6]The immune response to vaccination is divided into 6 stages (Figure 1), each of equal duration on average. The choice of 6 stages is justified by Appendix Figure 8.

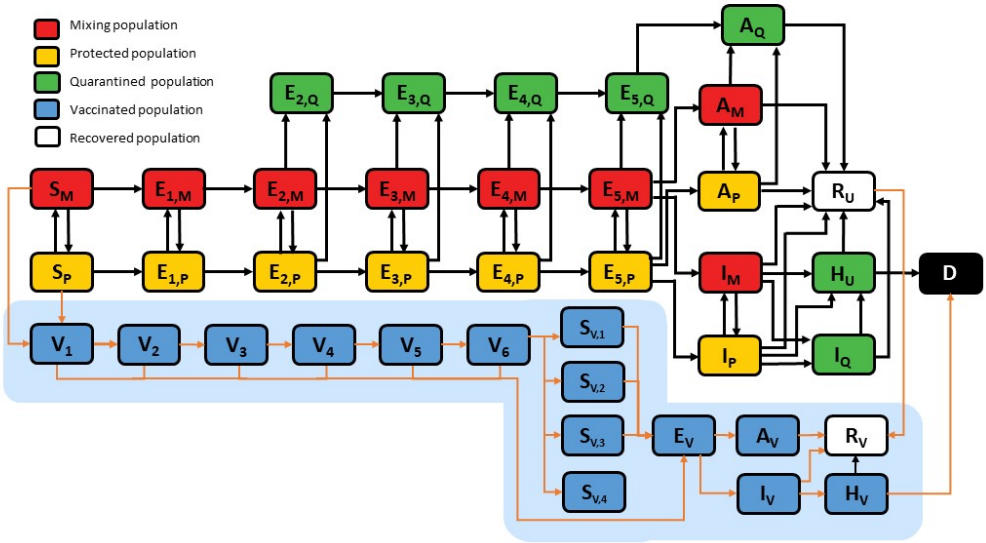

Figure 1. Illustration of compartmental model. The independent variable of the model is time t. The 40 dependent state variables of the model are populations, which are represented as boxes with rounded corners. A description of each state variable is given in Appendix Table 1. The 15 highlighted boxes (on the blue background) represent state variables introduced to capture the effects of vaccination and the Alpha and Delta variants. The other 25 boxes represent state variables considered in the model of Lin et al. *(5)*. Arrows connecting boxes represent transitions. Each transition represents the movement of persons from one population to another. Orange arrows represent transitions introduced to capture the effects of vaccination and the Alpha and Delta variants. Other arrows represent transitions considered in the model of Lin et al. *(5)*. Each arrow is associated with one or more parameters that characterize a rate of movement; these parameters are not shown here but are shown in Appendix Figure 1. A full description of

467 the model is given in the Appendix. Briefly, new parts of the model can be described as follows.
468 Vaccination is modeled by moving recovered unvaccinated persons (in the R_U population) into
469 the R_V population and susceptible persons (in the S_M and S_P populations) into the V_1 population.
470 The rate of vaccination changes from day to day to match the empirical daily rate of vaccination.
471 Recovered and susceptible persons have the same *per capita* probability of vaccination. Persons
472 in S_M are mixing (i.e., not practicing social distancing) and persons in S_P are practicing social
473 distancing (and thereby protected from infection to a degree). The series of transitions involving
474 the populations $V_1, \ldots, V_6$ was introduced to model the immune response to vaccination (i.e., the
475 amount of time required for vaccination to induce neutralizing antibodies). With this approach,
476 the time from vaccination to appearance of neutralizing antibodies is a random variable
477 characterized by an Erlang distribution. Persons in $V_1, \ldots, V_6$ may be infected. Persons in V_6
478 transition to one of the following four populations: $S_{V,1}, \ldots, S_{V,4}$. These populations represent
479 persons with varying degrees of immune protection. Persons in $S_{V,1}$ are not protected against
480 productive infection (i.e., an infection that can be transmitted to others) by any viral strain.
481 Persons in $S_{V,2}$ are protected against productive infection by viral strains present before the
482 emergence of Alpha but not Alpha or Delta. Persons in $S_{V,3}$ are protected against productive
483 infection by viral strains present before the emergence of Alpha and also Alpha but not Delta.
484 Persons in $S_{V,4}$ are protected against productive infection by all of the viral strains considered.
485 Vaccinated persons who become infected move into E_V. The time spent in E_V corresponds to the
486 length of the incubation period for vaccinated persons. The mean duration of the incubation
487 period is taken to be the same for vaccinated and unvaccinated persons; however, as a
488 simplification, for vaccinated persons, the time spent in the incubation period is exponentially
489 distributed (vs. Erlang distributed for unvaccinated persons). All non-quarantined exposed

persons (in populations E_V and $E_{i,M}$ and $E_{i,P}$ for $i = 1, \ldots, 5$) are taken to be infectious. Persons exiting E_V leave the incubation period and enter the immune clearance phase of infection, during which they may be asymptomatic (A_V) or symptomatic with mild disease (I_V). All non-quarantined asymptomatic persons (in populations A_V, A_M, and A_P) are taken to be infectious. Persons in A_V are all assumed to eventually recover (i.e., to enter R_V). Persons with mild symptomatic disease may recover (i.e., enter R_V) or experience severe disease, at which point they move to H_V (in hospital or isolated at home). Vaccinated persons have a diminished probability of severe disease in comparison to unvaccinated persons. Persons in H_V either recover (move to R_V) or die (move to D). For a person with severe disease, the probability of death is independent of vaccination status. We assume that vaccinated persons do not participate in social distancing, quarantine, or self-isolation driven by symptom awareness.

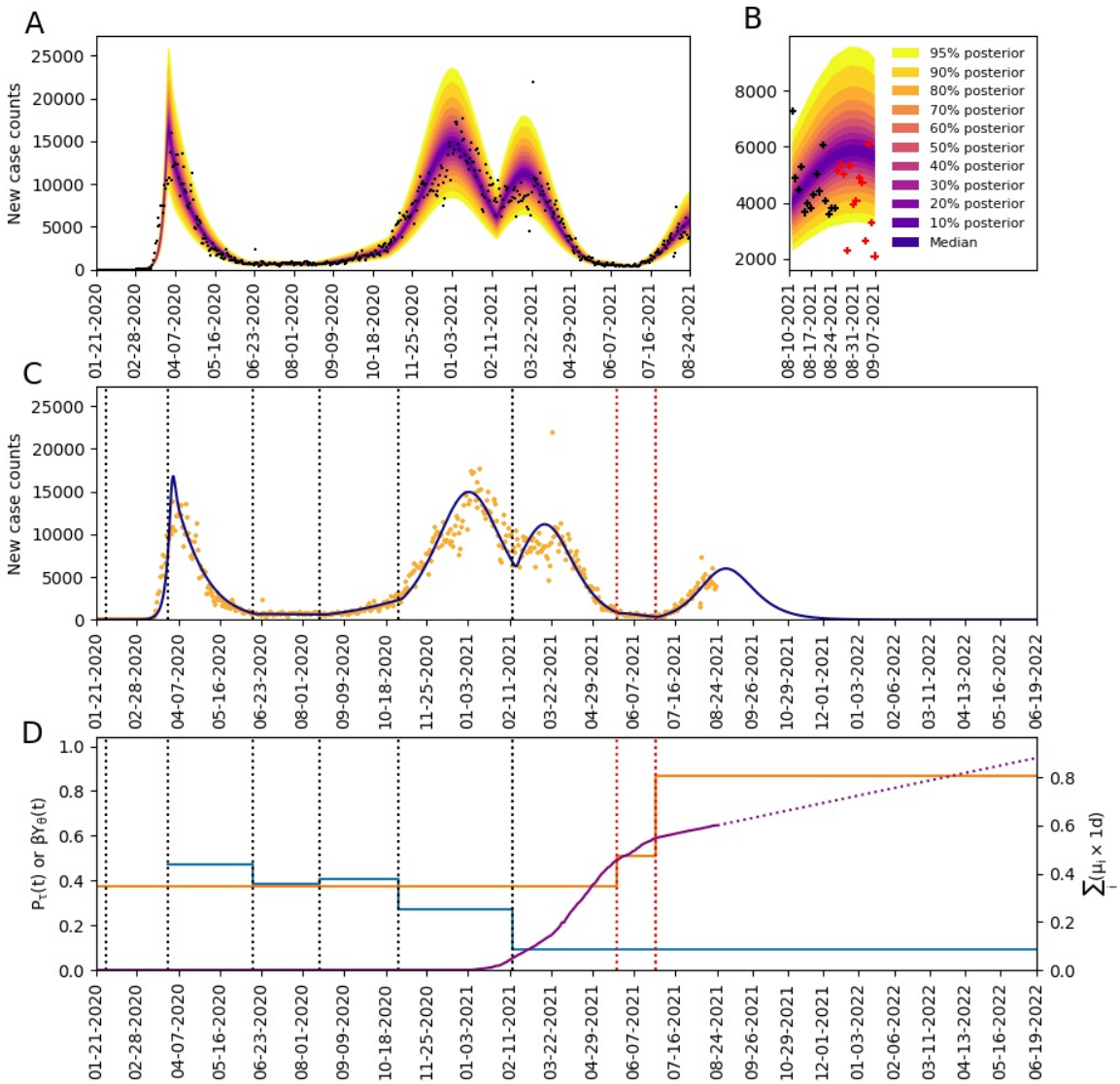

Figure 2. Inference results obtained for the New York City metropolitan statistical area (MSA) using regional surveillance data—daily reports of new COVID-19 cases—available for January 21, 2020 to August 24, 2021. A) Credible intervals of the time-dependent posterior predictive

distribution for detected and reported new cases are shown by color as indicated in the legend of panel (B) for each indicated date. The entire shaded region indicates the 95% credible interval. This region should cover approximately 95% of the data. Empirical case reports are indicated by black points. It should be noted that a single anomalous empirical case count above the upper range of the vertical axis is not shown. B) A 14-d ahead forecast with Bayesian uncertainty quantification. The last prediction date is September 7, 2021. As in panel (A), credible intervals of the posterior predictive distribution for detected and reported cases are shown by color as indicated in the legend. Empirical case reports are indicated by plus signs. Black plus signs indicate a subset of in-sample data used in inference from 14 days before the forecast date, and red plus signs indicate out-of-sample data (i.e., data not used in inference) from 14 days after the forecast date. C) The maximum likelihood prediction of daily number of new cases detected and reported. In this panel, the prediction has been extended to 300-d beyond the date of inference (under the assumption of vaccination at the average daily rate between August 5, 2021 and August 24, 2021). Empirical case reports are indicated by orange points. The black vertical broken lines indicate the dates on which social-distancing parameters changed in the model. The red vertical broken lines indicate the inferred variant takeover times. The left line indicates the Alpha takeover time, and the right line indicates the Delta takeover time. D) The social-distancing quasi-stationary setpoint given by $P_\tau(t)$ (blue curve), the disease transmissibility rate constant given by $\beta Y_\theta(t)$ (orange curve), and the sum $\sum_i(\mu_i \times 1\ \mathrm{d})$ (purple curve), which is the cumulative fraction of the population that has been vaccinated, are shown as a function of time t. Note that the value of $P_\tau(t)$ is dimensionless and the that the value of $\beta Y_\theta(t)$ has units of d^{-1}. An initial social-distancing period begins at time $t = \sigma$. During this period, the quasi-stationary setpoint (the fraction of the susceptible population practicing social distancing) is $p_0 = 0.47$. The

initial social-distancing period is followed by four distinct social-distancing periods, with quasi-stationary setpoints given by the step function $P_\tau(t)$. As indicated, the values of $P_\tau(t)$ are $p_1 = 0.39$ for $t \in [\tau_1, \tau_2)$, $p_2 = 0.41$ for $t \in [\tau_2, \tau_3)$, $p_3 = 0.27$ for $t \in [\tau_3, \tau_4)$, and $p_4 = 0.09$ for $t \in [\tau_4, \infty)$. The times σ, τ_1, τ_2, τ_3, and τ_4 are indicated by vertical broken black lines. The quantity $\beta Y_\theta(t)$ characterizes the rate of disease transmission at time t. The value of $Y_\theta(t)$, a step function, is the variant transmissibility factor. The initial value of $Y_\theta(t)$ is 1. As indicated, the values of $\beta Y_\theta(t)$ are 0.37 for $t \in [0, \theta_1)$, 0.51 for $t \in [\theta_1, \theta_2)$, and 0.87 for $t \in [\theta_2, \infty)$. These values correspond to the following transmissibility factors for Alpha and Delta: $y_1 = 1.37$ and $y_2 = 2.33$. The times θ_1 and θ_2 are indicated by vertical broken red lines. The solid part of the magenta curve indicates the empirical cumulative number of completed vaccinations, and the broken part of the magenta curve indicates the projected cumulative number of vaccinations completed if vaccinations continue at the average daily rate between August 5, 2021 and August 24, 2021.

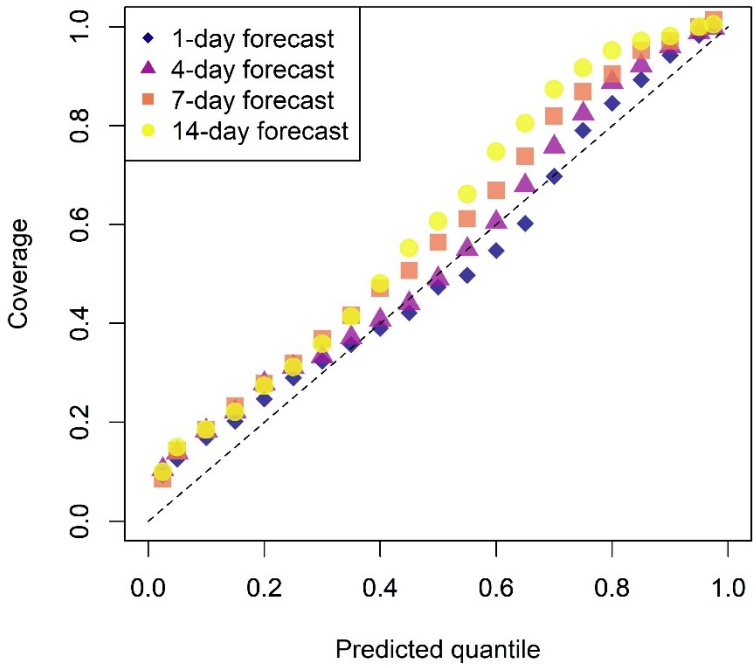

Figure 3. Accuracy of forecasts of number of new cases detected for the 15 most populous metropolitan statistical areas (MSAs) in the United States from July 15, 2021 to August 24, 2021 assessed using out-of-sample data. We considered all available case counts for the 15 MSAs over the period of interest and corresponding 1-, 4-, 7-, and 14-d ahead posterior predictive distributions. The coverage was calculated as explained in the Appendix.

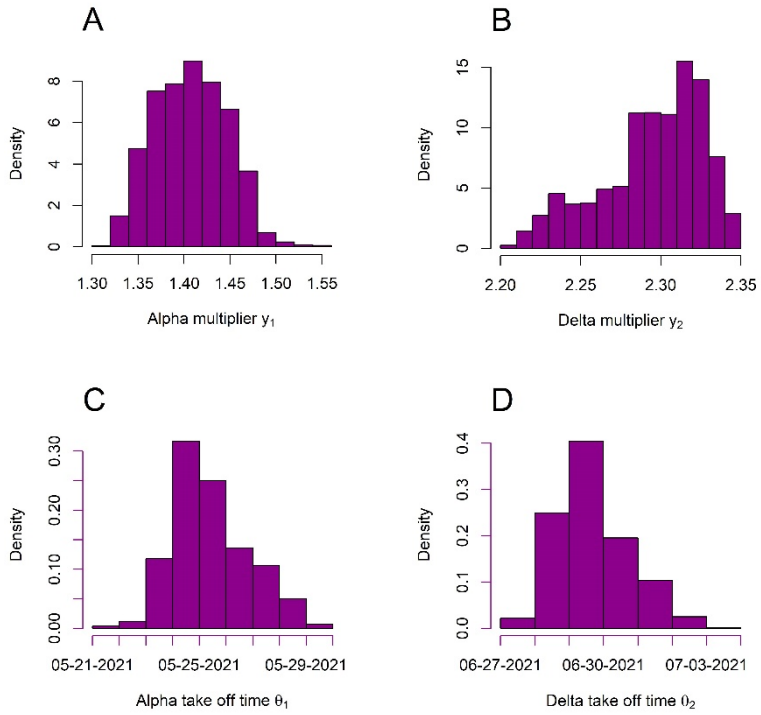

Figure 4. Marginal posteriors for A) the Alpha transmissibility factor y_1, B) the Delta transmissibility factor y_2, C) the Alpha takeover time θ_1, and D) the Delta takeover time θ_2. The transmissibility factors characterize the increased infectiousness of SARS-CoV-2 variants Alpha (lineage B.1.1.7) and Delta (lineage.1.617.2) in comparison to pre-existing viral strains, i.e., strains in circulation before the emergence of Alpha. Each takeover time is the time at which a variant (Alpha or Delta) became the dominant viral strain. Time $t = 0$ corresponds to midnight on January 21, 2020. Marginal posteriors are shown as histograms and are derived from parameter posterior samples obtained for the New York City metropolitan statistical area using surveillance data available from January 21, 2020 to August 24, 2021.

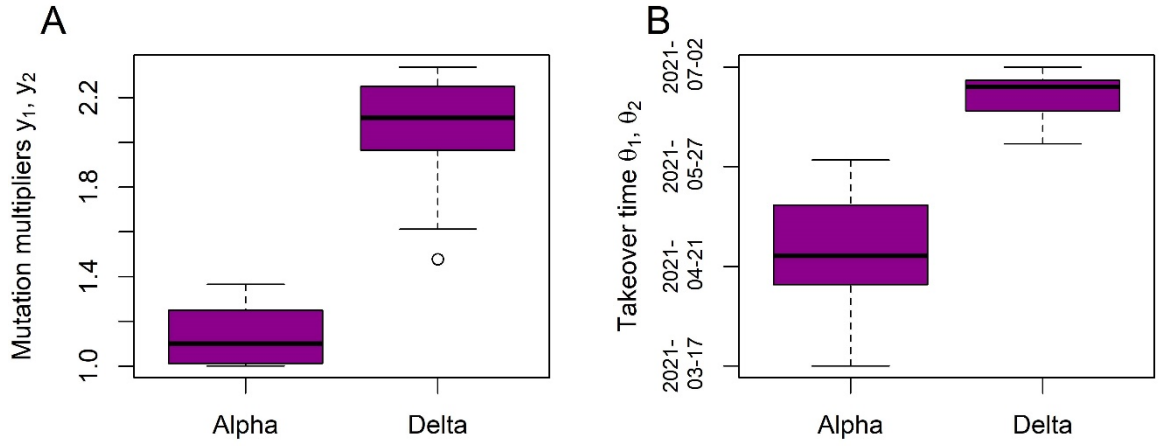

Figure 5. Box plot summaries of the maximum *a posteriori* (MAP) estimates of A) y_1 and y_2 and B) θ_1 and θ_2 obtained for each of the 15 most populous metropolitan statistical areas (MSAs) in the United States using MSA-specific surveillance data available from January 21, 2020 to August 24, 2021. As indicated, the mean MAP estimates of y_1 and y_2 are 1.2 and 2.l, and the mean MAP estimates of θ_1 and θ_2 are 464 d and 517 d, which correspond to May 2, 2021 and June 23, 2021. Time $t = 0$ corresponds to midnight on January 21, 2020. Recall that y_1 (y_2) quantifies the infectiousness of Alpha (Delta) relative to strains circulating before the emergence of Alpha and that θ_1 (θ_2) is the Alpha (Delta) takeover time.

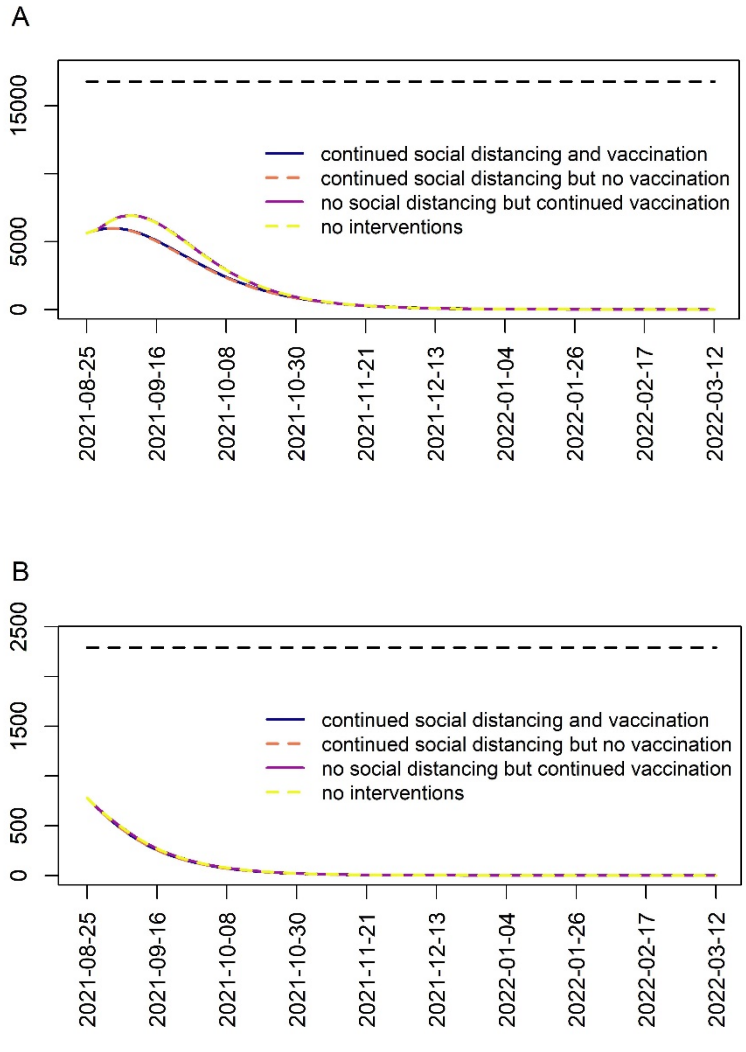

Figure 6. Projected daily detection of new COVID-19 cases in the face of Delta over a 300-d period (August 24, 2021 to March 12, 2022) for A) the New York city metropolitan statistical area (MSA) and B) the San Francisco MSA. Projections are based on Delta remaining the predominant circulating viral strain and the maximum likelihood parameter estimates obtained using MSA-specific surveillance data available from January 21, 2020 to August 24, 2021 (e.g.,

the parameter values given in Table 1 for the New York City MSA), except as noted below. In each panel, four scenarios are considered: continued social distancing as on August 24, 2021 and vaccination at a daily rate equal to the average empirical daily rate over the 20-d period starting on August 5, 2021 and ending on August 24, 2021 (dark blue curve), continued social distancing but no vaccination (orange curve), no social distancing but continued vaccination (violet curve) and no interventions (yellow curve). The black horizontal dashed line indicates the largest MAP estimate for number of new cases detected over any 1-d period.

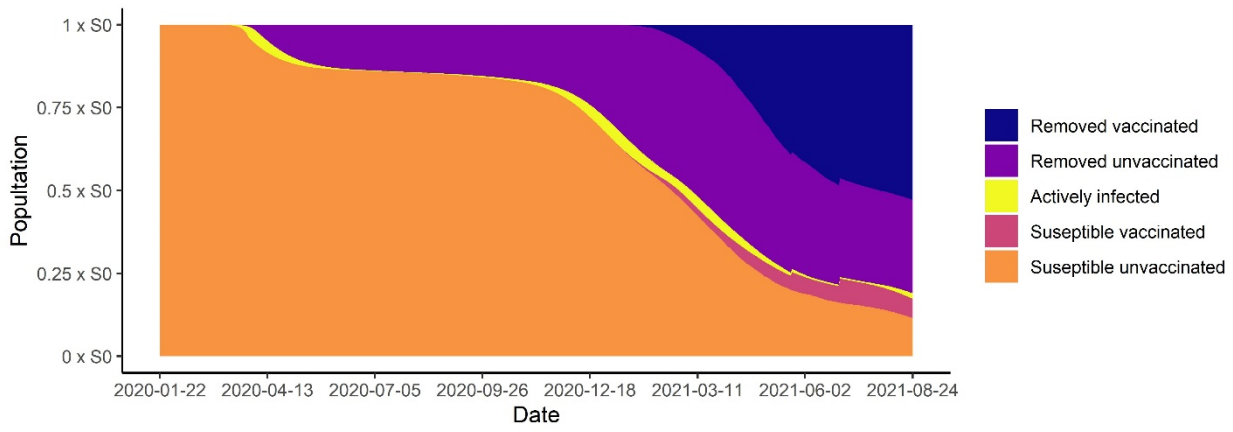

Figure 7. Inferred changes in the distribution of persons amongst five selected populations over the course of the local COVID-19 epidemic in the New York City metropolitan statistical area. The five populations sum to a constant, S_0, the total population. Results shown here are based on the parameter values given in Tables 1 and 2. The five populations are defined as follows: the population of susceptible unvaccinated persons (orange area) is given by $S_M + S_P$, the population of susceptible vaccinated persons (pink area) is given by $\sum_{i=1}^{6} V_i + S_{V,1} + U_{\theta_1}(t)S_{V,2} + U_{\theta_2}(t)S_{V,3}$, the population of actively infected persons (yellow area) is given by $H_U + H_V + E_V + \sum_{i=1}^{5}\left(E_{i,M} + E_{i,P} + E_{i,Q}\right) + \sum_{x\in\{M,P,Q,V\}}(A_x + I_x)$, the population of removed unvaccinated persons (magenta area) is given by $R_U + D$, and the population of removed vaccinated persons (blue area) is given by $R_V + (1 - U_{\theta_1}(t))S_{V,2} + (1 - U_{\theta_2}(t))S_{V,3} + S_{V,4}$. Except for $U_{\theta_1}(t)$ and $U_{\theta_2}(t)$, the terms in the above definitions refer to state variables of the compartmental model of Figure 1, which are defined in Appendix Table 1. $U_{\theta_1}(t)$ and $U_{\theta_2}(t)$ are unit step functions, which change value from 0 to 1 at time $t = \theta_1$ and $t = \theta_2$, respectively. Recall that θ_1 and θ_2 are the Alpha and Delta takeover times.

Appendix Text

List of Metropolitan Statistical Areas of Interest

As in the study of Lin et al. *(1)*, we considered the 15 most populous metropolitan statistical areas (MSAs) in the United States (US). These MSAs, which are delineated by the US Office of Management and Budget *(2)*, encompass the following cities (listed in order of MSA population from greatest to least): New York City, New York; Los Angeles, California; Chicago, Illinois; Dallas, Texas; Houston, Texas; Washington, District of Columbia; Miami, Florida; Philadelphia, Pennsylvania; Atlanta, Georgia; Phoenix, Arizona; Boston, Massachusetts; San Francisco, California; Riverside, California; Detroit, Michigan; and Seattle, Washington.

Imputation of Missing Daily Case Counts

As of August 24, 2021, many regions in the US are not reporting new detected COVID-19 cases on a strictly daily basis. When one or more daily case counts are not available, we impute daily case counts on the basis of a linear fit to the two nearest available cumulative case counts. This approach has the effect of evenly distributing case counts across the days for which daily reports are unavailable.

Equations of the Compartmental Model

The compartmental model, which is illustrated in Figure 1 and Appendix Figure 1, consists of the following 40 ordinary differential equations (ODEs):

$$\frac{dS_M}{dt} = -\beta Y_\theta(t)\left(\frac{S_M}{S_0}\right)\left(\phi_M(t,\rho) + m_b\phi_P(t,\rho)\right) \tag{1}$$

$$- U_\sigma(t)\Lambda_\tau(t)\left[P_\tau(t)S_M - \left(1 - P_\tau(t)\right)S_P\right] - \mu(t)S_0\left(\frac{S_M}{\phi_V(t)}\right)$$

$$\frac{dS_P}{dt} = -m_b\beta Y_\theta(t)\left(\frac{S_P}{S_0}\right)\left(\phi_M(t,\rho) + m_b\phi_P(t,\rho)\right) \tag{2}$$

$$+ U_\sigma(t)\Lambda_\tau(t)\left[P_\tau(t)S_M - \left(1 - P_\tau(t)\right)S_P\right] - \mu(t)S_0\left(\frac{S_P}{\phi_V(t)}\right)$$

$$\frac{dE_{1,M}}{dt} = \beta Y_\theta(t)\left(\frac{S_M}{S_0}\right)(\phi_M(t,\rho) + m_b\phi_P(t,\rho)) - k_L E_{1,M} \tag{3}$$

$$- U_\sigma(t)\Lambda_\tau(t)\left[P_\tau(t)E_{1,M} - (1 - P_\tau(t))E_{1,P}\right]$$

$$\frac{dE_{1,P}}{dt} = m_b\beta Y_\theta(t)\left(\frac{S_P}{S_0}\right)(\phi_M(t,\rho) + m_b\phi_P(t,\rho)) - k_L E_{1,P} \tag{4}$$

$$+ U_\sigma(t)\Lambda_\tau(t)\left[P_\tau(t)E_{1,M} - (1 - P_\tau(t))E_{1,P}\right]$$

$$\frac{dE_{i,M}}{dt} = k_L E_{i-1,M} - k_L E_{i,M} - k_Q E_{i,M} - U_\sigma(t)\Lambda_\tau(t)\left[P_\tau(t)E_{i,M} - (1 - P_\tau(t))E_{i,P}\right], \tag{5}$$

$$\text{for } i = 2, 3, 4, 5$$

$$\frac{dE_{i,P}}{dt} = k_L E_{i-1,P} - k_L E_{i,P} - k_Q E_{i,P} + U_\sigma(t)\Lambda_\tau(t)\left[P_\tau(t)E_{i,M} - (1 - P_\tau(t))E_{i,P}\right], \tag{6}$$

$$\text{for } i = 2, 3, 4, 5$$

$$\frac{dE_{2,Q}}{dt} = k_Q(E_{2,M} + E_{2,P}) - k_L E_{2,Q} \tag{7}$$

$$\frac{dE_{i,Q}}{dt} = k_Q\left(E_{i,M} + E_{i,P}\right) + k_L E_{i-1,Q} - k_L E_{i,Q}, \text{ for } i = 3, 4, 5 \tag{8}$$

$$\frac{dA_M}{dt} = f_A k_L E_{5,M} - k_Q A_M - U_\sigma(t)\Lambda_\tau(t)[P_\tau(t)A_M - (1 - P_\tau(t))A_P] - c_A A_M \tag{9}$$

$$\frac{dA_P}{dt} = f_A k_L E_{5,P} - k_Q A_P + U_\sigma(t)\Lambda_\tau(t)[P_\tau(t)A_M - (1 - P_\tau(t))A_P] - c_A A_P \tag{10}$$

$$\frac{dA_Q}{dt} = f_A k_L E_{5,Q} + k_Q(A_M + A_P) - c_A A_Q \tag{11}$$

$$\frac{dI_M}{dt} = (1 - f_A)k_L E_{5,M} - \left(k_Q + j_Q\right)I_M - U_\sigma(t)\Lambda_\tau(t)\left[P_\tau(t)I_M - \left(1 - P_\tau(t)\right)I_P\right] - c_I I_M \tag{12}$$

$$\frac{dI_P}{dt} = (1 - f_A)k_L E_{5,P} - \left(k_Q + j_Q\right)I_P + U_\sigma(t)\Lambda_\tau(t)[P_\tau(t)I_M - \left(1 - P_\tau(t)\right)I_P] - c_I I_P \tag{13}$$

$$\frac{dI_Q}{dt} = (1 - f_A)k_L E_{5,Q} + \left(k_Q + j_Q\right)(I_M + I_P) - c_I I_Q \tag{14}$$

$$\frac{dH_U}{dt} = f_H c_I\left(I_M + I_P + I_Q\right) - c_H H_U \tag{15}$$

$$\frac{dD}{dt} = (1 - f_R)c_H H_U + (1 - f_R)c_H H_V \tag{16}$$

$$\frac{dR_U}{dt} = c_A\left(A_M + A_P + A_Q\right) + (1 - f_H)c_I\left(I_M + I_P + I_Q\right) + f_R c_H H_U - \mu(t)S_0\left(\frac{R_U}{\phi_V(t)}\right) \tag{17}$$

$$\frac{dV_1}{dt} = \mu(t)S_0\left(\frac{S_M + S_P}{\phi_V(t)}\right) - k_V V_1 - \beta Y_\theta(t)\left(\frac{V_1}{S_0}\right)\left(\phi_M(t,\rho) + m_b\phi_P(t,\rho)\right) \tag{18}$$

$$\frac{dV_i}{dt} = k_V V_{i-1} - k_V V_i - \beta Y_\theta(t)\left(\frac{V_i}{S_0}\right)\left(\phi_M(t,\rho) + m_b\phi_P(t,\rho)\right), \tag{19}$$

for $i = 2, 3, 4, 5, 6$

$$\frac{dS_{V,1}}{dt} = (1 - f_0)k_V V_6 - \beta Y_\theta(t)\left(\frac{S_{V,1}}{S_0}\right)\left(\phi_M(t,\rho) + m_b\phi_P(t,\rho)\right) \tag{20}$$

$$\frac{dS_{V,2}}{dt} = (f_0 - f_1)k_V V_6 - U_{\theta_1}(t)\beta Y_\theta(t)\left(\frac{S_{V,2}}{S_0}\right)\left(\phi_M(t,\rho) + m_b\phi_P(t,\rho)\right) \tag{21}$$

$$\frac{dS_{V,3}}{dt} = (f_1 - f_2)k_V V_6 - U_{\theta_2}(t)\beta Y_\theta(t)\left(\frac{S_{V,3}}{S_0}\right)\left(\phi_M(t,\rho) + m_b\phi_P(t,\rho)\right) \tag{22}$$

$$\frac{dS_{V,4}}{dt} = f_2 k_V V_6 \tag{23}$$

$$\frac{dE_V}{dt} = \beta Y_\theta(t)\left(\frac{1}{S_0}\right)\left(\phi_M(t,\rho) + m_b\phi_P(t,\rho)\right) \cdot \sum_{i=1}^{6}\left(V_i + S_{V,1} + U_{\theta_1}(t)S_{V,2} + U_{\theta_2}(t)S_{V,3}\right) - \left(\frac{k_L}{5}\right)E_V \tag{24}$$

$$\frac{dA_V}{dt} = f_A\left(\frac{k_L}{5}\right)E_V - c_A A_V \tag{25}$$

$$\frac{dI_V}{dt} = (1 - f_A)\left(\frac{k_L}{5}\right)E_V - c_I I_V \tag{26}$$

$$\frac{dH_V}{dt} = m_h f_H c_I I_V - c_H H_V \tag{27}$$

$$\frac{dR_V}{dt} = \mu(t)S_0\left(\frac{R_U}{\phi_V(t)}\right) + c_A A_V + (1 - m_h f_H)c_I I_V + f_R c_H H_V \tag{28}$$

In these equations, the independent variable is time t, and the state variables (S_M, S_P, $E_{1,M}, \ldots, E_{5,M}$, $E_{1,P}, \ldots, E_{5,P}$, $E_{2,Q}, \ldots, E_{5,Q}$, A_M, A_P, A_Q, I_M, I_P, I_Q, H_U, D, R_U, $V_1, \ldots, V_6$, $S_{V,1}, \ldots, S_{V,4}$, E_V, A_V, I_V, H_V, and R_V) represent 40 (sub)populations (Appendix Table 1), which change over time. Thus, each ODE in Equations (1)–(28) defines the time-rate of change of a

population, i.e., the time-rate of change of a state variable. Note that Equations (5), (6), (8) and (19) define 4, 4, 3, and 5 ODEs of the model, respectively. The model is formulated such that S_0, the total population, is constant. Thus, the model does not account for birth, death for reasons other than COVID-19, or migration (in or out of the population).

The initial condition associated with Equations (1)–(28) is taken to be $S_M(t_0) = S_0$, $I_M(t_0) = I_0 = 1$, with all other populations (S_P, $E_{1,M}, \dots, E_{5,M}$, $E_{1,P}, \dots, E_{5,P}$, $E_{2,Q}, \dots, E_{5,Q}$, A_M, A_P, A_Q, I_P, I_Q, H_U, D, R_U, $V_1, \dots, V_6$, $S_{V,1}, \dots, S_{V,4}$, E_V, A_V, I_V, H_V, and R_V) equal to 0. Recall that the parameter S_0 denotes the total region-specific population size. Thus, we assume that the entire population is susceptible at the start of the local epidemic at time $t = t_0$>0, where time $t = 0$ corresponds to 0000 hours (midnight) on January 21, 2020. The parameter I_0 denotes the number of infectious symptomatic persons at the start of the regional epidemic.

In the model, the parameters β, k_L, k_Q, j_Q, c_A, c_I, c_H, and k_V are positive-valued rate constants (all with units of d^{-1}), and the parameters m_b, m_h, f_A, f_H, f_R, $f_0 \geq f_1$, $f_1 \geq f_2$, and f_2 are (dimensionless) fractions. Brief definitions of parameters are given in Tables 1 and 2.

In the model, the quantities $\phi_M(t, \rho)$, $\phi_P(t, \rho)$, and $\phi_V(t)$ are functions of (time-dependent) state variables (as defined below), which represent the population of infectious persons who are mixing freely (i.e., not practicing social distancing), the population of infectious persons who are practicing social distancing, and the population of persons eligible for vaccination, respectively. The quantities $\phi_M(t, \rho)$ and $\phi_P(t, \rho)$ are also functions of $\rho \equiv (\rho_E, \rho_A)$, where ρ_E (ρ_A) is a dimensionless ratio representing the infectiousness of persons in the incubation phase of infection (the infectiousness of asymptomatic persons in the immune clearance phase of infection) relative to the infectiousness of symptomatic persons with the same

social-distancing behavior. The quantity $\phi_V(t)$ represents the population of persons eligible for vaccination.

$$\phi_M(t,\rho) = I_M + I_V + \rho_E\left(E_{2,M} + E_{3,M} + E_{4,M} + E_{5,M} + E_V\right) + \rho_A(A_M + A_V) \tag{29}$$

$$\phi_P(t,\rho) = I_P + \rho_E\left(E_{2,P} + E_{3,P} + E_{4,P} + E_{5,P}\right) + \rho_A A_P \tag{30}$$

$$\phi_V(t) = S_M + S_P + \sum_{i=1}^{5}\left(E_{i,M} + E_{i,P}\right) + A_M + A_P + R_U \tag{31}$$

The state variables that appear in these equations represent time-varying populations. Recall that state variables are defined in Appendix Table 1.

In the model, the quantities $U_\sigma(t)$, $U_{\theta_1}(t)$, and $U_{\theta_2}(t)$ are unit step functions. The values of these functions change from 0 to 1 at the times indicated by the subscripts: σ, the onset time of the initial social-distancing period; θ_1, the takeover time of SARS-CoV-2 variant Alpha; and θ_2, the takeover time of SARS-CoV-2 variant Delta.

$$U_\sigma(t) = \begin{cases} 0 & t < \sigma \\ 1 & t \geq \sigma \end{cases} \tag{32}$$

$$U_{\theta_1}(t) = \begin{cases} 0 & t < \theta_1 \\ 1 & t \geq \theta_1 \end{cases} \tag{33}$$

$$U_{\theta_2}(t) = \begin{cases} 0 & t < \theta_2 \\ 1 & t \geq \theta_2 \end{cases} \tag{34}$$

As indicated in Appendix Figure 1, transitions from S_M to S_P, for example, become possible at time $t = \sigma$, transitions from $S_{V,2}$ to E_V become possible at time $t = \theta_1$, and transitions from $S_{V,3}$ to E_V become possible at time $t = \theta_2$.

In the model, the quantities $P_\tau(t)$, and $\Lambda_\tau(t)$ are step functions that characterize changes in social distancing. The value of $P_\tau(t)$ determines a setpoint steady-state fraction of susceptible persons who are practicing social distancing. The value of $\Lambda_\tau(t)$ determines a time scale for approach to the setpoint steady state. Changes in the values of $P_\tau(t)$ and $\Lambda_\tau(t)$ occur coordinately. These changes occur at times $t = \tau_1, \dots, \tau_n$, where n is the number of distinct social-distancing periods beyond an initial social-distancing period. Initially, $n = 0$. The value of n is incremented by 1 (at an inferred time) if $n \leftarrow n + 1$ is determined to be admissible by a model-selection procedure *(1)*, which is described below. It should be noted that $p_0, p_1, \dots, p_n$ are parameters of $P_\tau(t)$ and that $\lambda_0, \lambda_1, \dots, \lambda_n$ are parameters of $\Lambda_\tau(t)$. These parameters determine the values of the step functions over different periods. For example, for $n = 1$, p_1 is the value of $P_\tau(t)$ and λ_1 is the value of $\Lambda_\tau(t)$ for the period $t \in [\tau_1, \tau_2)$.

$$P_\tau(t) = \begin{cases} p_0 & \sigma \leq t < \tau_1 \\ p_1 & \tau_1 \leq t < \tau_2 \\ \vdots & \vdots \\ p_n & \tau_n \leq t < \infty \end{cases} \tag{35}$$

$$\Lambda_\tau(t) = \begin{cases} \lambda_0 & \sigma \leq t < \tau_1 \\ \lambda_1 & \tau_1 \leq t < \tau_2 \\ \vdots & \vdots \\ \lambda_n & \tau_n \leq t < \infty \end{cases} \tag{36}$$

In the model, the quantity $\mu(t)$ is a step function that characterizes the current rate of vaccination. The value of $\mu(t)$ is determined by the empirical daily rate of vaccination, and thus, can vary (up or down) from day to day. Vaccination data were extracted daily from Covid Act Now using the Covid Act Now Data API *(3)*. We will use μ_i to refer to the value of $\mu(t)$ for $t \in [t_i, t_{i+1})$, where time t_i corresponds to midnight on the ith day after January 21, 2020.

$$\mu(t) = \mu_i \text{ for } t \in [t_i, t_{i+1}) \tag{37}$$

Settings for μ_i were made such that $\mu_i S_0 \times 1$ d corresponds to the number of vaccinations completed in the nearest past 1-d period according to Covid Act Now data.

In the model, the quantity $Y_\theta(t)$ is a step function that quantifies how disease transmissibility increases upon emergence of SARS-CoV-2 variants Alpha and Delta. Initially, $Y_\theta(t) = 1$. The value of $Y_\theta(t)$ is increased (by an inferred factor greater than 1 at an inferred time, θ_1 or θ_2) if the change is determined to be admissible by a model-selection procedure, which is described below. It should be noted that y_1 and y_2 are parameters of $Y_\theta(t)$. These parameters determine the values of the step function $Y_\theta(t)$ over different periods: y_1 is the value of $Y_\theta(t)$ for the period $t \in [\theta_1, \theta_2)$ and y_2 is the value of $Y_\theta(t)$ for the period $t \in [\theta_2, \infty)$ or until a new variant supplants Delta as the dominant circulating viral strain.

$$Y_\theta(t) = \begin{cases} y_0 & \theta_0 \leq t < \theta_1 \\ y_1 & \theta_1 \leq t < \theta_2 \\ \vdots & \vdots \\ y_m & \theta_m \leq t < \infty \end{cases} \tag{38}$$

where m is the number of viral variants that have emerged up to the current time, $\theta_0 \equiv t_0$, and $y_0 \equiv 1$. Here, we consider $m = 0, 1, 2$. The setting for m is determined through model selection, as alluded to above. In inferences, the time θ_1 was constrained to fall after December 31, 2020 (i.e., we constrained variant emergence to 2021).

Equations of the Auxiliary Measurement Model

As in the study of Lin et al. *(1)*, we assumed that only symptomatic persons are detected in testing. The accumulation of symptomatic persons is governed by

$$\frac{dC_S}{dt} = (1 - f_A)\left[k_L\left(E_{5,M} + E_{5,P} + E_{5,Q}\right) + \left(\frac{k_L}{5}\right)E_V\right] \tag{39}$$

where $C_S(t)$ is the cumulative number of symptomatic persons (cases) at time t. Here, unlike in the study of Lin et al. *(1)*, the expression for $C_S(t)$ accounts for exposed persons in quarantine. Initially, $C_S = 0$. We numerically integrated Appendix Equation (39) together with the ODEs of the compartmental model. From the trajectory for C_S, we derive a prediction for the expected number of new COVID-19 cases reported on calendar date $\mathcal{D}_\mathrm{i}$, $I(t_i, t_{i+1})$, using the following equation:

$$I(t_i, t_{i+1}) = f_D[C_S(t_{i+1}) - C_S(t_i)] \tag{40}$$

where f_D is an adjustable region-specific parameter characterizing the time-averaged fraction of symptomatic cases detected and reported, t_i corresponds to midnight on the ith day after January 21, 2020, and $t_{i+1} - t_i$ is the reporting interval (1 d). We compare $I(t_i, t_{i+1})$ to δC_i, the number of new cases reported on calendar date $\mathcal{D}_\mathrm{i}$.

Definition of the Likelihood Function

Bayesian inference relies on the definition of a likelihood, which here serves the purpose of measuring the compatibility of available surveillance data with adjustable (free) parameter values. Let us use $\{\delta C_i\}_{i=0}^{d}$ to denote the daily case reporting data available between 0 and d days after midnight on January 21, 2020 (the date of the first case report in the US), and let $D = \{\delta C_i\}_{i=0}^{d}$. Let us use $\theta_F(n, m)$ to denote the set of adjustable (free) parameter values. The number of adjustable parameters, $|\theta_F|$, depends on n, the number of social-distancing periods considered beyond an initial social-distancing period, and m, the number of SARS-CoV-2 variants under consideration. As in the study of Lin et al. *(1)*, we assume that δC_i, the number of

new COVID-19 cases detected over a 1-d period and reported on calendar date $\mathcal{D}_{\mathrm{i}}$ for a given region, is a random variable and its expected value follows a model-derived deterministic trajectory given by $I(t_i, t_{i+1})$ (Equation 40). We assume that day-to-day fluctuations in the random variable are independent and characterized by a negative binomial distribution $\mathrm{NB}(r, q_i)$, which has two parameters, $r > 0$ and $q_i \in (0,1)$. Note that $\mathbb{E}[\mathrm{NB}(r, q_i)] = r(1 - q_i)/q_i$. We assume that this distribution has the same dispersion parameter r across all case reports. With these assumptions, we arrive at the following likelihood function:

$$\mathcal{L}\left(\theta_F(n,m); \{\delta C_i\}_{i=0}^{d}\right) = \prod_{i=0}^{d} \log \mathcal{L}_i(\theta_F\,(n,m); \delta C_i) \tag{41}$$

where

$$\mathcal{L}_i(\theta_F(n,m); \delta C_i) = \mathrm{nbinom}(\delta C_i; r, q_i) = \binom{\delta C_i + r - 1}{\delta C_i - 1} q_i^r (1 - q_i)^{\delta C_i} \tag{42}$$

and

$$q_i = \frac{r}{r + I(t_i, t_{i+1})}. \tag{43}$$

In these equations, i is an integer indicating the date $\mathcal{D}_i$ and period (t_i, t_{i+1}); $\mathrm{nbinom}(\delta C_i; r, q_i)$ is the probability mass function of the negative binomial distribution $\mathrm{NB}(r, q_i)$, and $\theta_F(n,m) = \{t_0, \beta, \sigma, \tau_1, \dots, \tau_n, p_0, p_{1,} \dots, p_n, \lambda_0, \lambda_1, \dots, \lambda_n, \theta_1, \dots, \theta_m, y_1, \dots, y_m, f_D, r\}$ for $n \geq 1$ and $m \geq 1$. $\theta_F(0,0) = \{t_0, \beta, p_0, \lambda_0, f_D, r\}$.

Parameters

Each model parameter is briefly described in Tables 1 and 2. These parameters have either fixed values or adjustable values (i.e., values inferred from surveillance data). The fixed values may be universal (i.e., applicable to all MSAs of interest) or MSA-specific. All inferred parameter values are MSA-specific. In addition, the measurement model (Appendix Equations 39 and 40) has one adjustable MSA-specific parameter, f_D, and the likelihood function (Appendix Equations 41–43) has one adjustable MSA-specific parameter, r. Values of the other likelihood parameters, $q_0, \ldots, q_d$, are constrained and are determined using Appendix Equation 43.

The model shares $19 + 3n$ parameters with the model of Lin et al. *(1)*, including parameters that define the initial condition (t_0, I_0, and S_0). (Recall that n is the number of social-distancing periods being considered beyond the initial social-distancing period.) The shared parameters are t_0, I_0, S_0, β, σ, $\tau_1, \ldots, \tau_n$, $p_0, \ldots, p_n$, $\lambda_0, \ldots, \lambda_n$, ρ_A, ρ_E, m_b, f_A, f_H, f_R, k_L, k_Q, j_Q, c_A, c_H, and c_I. As in the study of Lin et al. *(1)*, we inferred MSA-specific values for the following parameters: t_0, β, σ, $p_0, \ldots, p_n$, and $\lambda_0, \ldots, \lambda_n$. We also inferred MSA-specific values for $\tau_1, \ldots, \tau_n$ provided that $n \geq 1$. As in the study of Lin et al. *(1)*, the remaining 14 parameters shared between the old and new models (I_0, S_0, ρ_A, ρ_E, m_b, f_A, f_H, f_R, k_L, k_Q, j_Q, c_A, c_H, and c_I) were taken to have fixed values, and we adopted the settings of Lin et al. *(1)* for these parameters (Table 2). These settings are universal except for the setting for S_0, the total population, which is MSA-specific.

Our extension of the model of Lin et al. *(1)* introduces $5 + 2(m + 1) + (d + 1)$ parameters, where m (= 0, 1 or 2) is the number of SARS-CoV-2 variants being considered and d is the number of days since January 21, 2020: $\theta_0, \ldots, \theta_m$, $y_0, \ldots, y_m$, m_h, f_0, f_1, f_2, k_V, and

144 $\mu_0, \ldots, \mu_d$. The θ and y parameters are variant takeover times and transmissibility factors,
145 respectively, except that the value of θ_0 is defined as t_0 and the value of y_0 is defined as 1. The
146 Alpha transmissibility factor y_1, the Alpha takeover time θ_1, the Delta transmissibility factor y_2,
147 and the Delta takeover time θ_2 were (eventually) inferred for each MSA once model selection
148 permitted consideration of $m = 2$ (cf. Table 1). The transmissibility factors were each
149 constrained to be greater than or equal to 1. We constrained θ_1 to fall after December 31, 2020
150 and θ_2 to fall after θ_1. The settings for $\mu_0, \ldots, \mu_d$ are empirical and MSA-specific. Each μ_i is set
151 such that $\mu_i S_0 \times 1$ d is the number of vaccinations completed over the past 1-d period nearest to
152 the ith day after January 21, 2020. As noted earlier, the number of completed vaccinations was
153 obtained for each MSA from Covid Act Now using the Covid Act Now Data API *(3)*. In the
154 spreadsheet downloaded daily, the 'metrics.vaccinationsCompletedRatio' column gives the
155 percentage of the total population that has received the recommended number of shots: one shot
156 for Ad26.CoV2.S (Janssen, Johnson & Johnson) or two shots for mRNA-1273 (Moderna) and
157 BNT162b2 (Pfizer-BioNTech). As a simplification, we considered all completed vaccinations to
158 be equivalent. The parameters m_h, f_0, f_1, f_2, and k_V were assigned fixed universal estimates
159 (Table 2). Each of these estimates is explained below.

160 The rate constant k_V characterizes the rate of transition out of compartment V_i for $i =$
161 $1, \ldots, n_V$. Recall that, in the model, susceptible persons enter V_1 upon vaccination (Figure 1,
162 Appendix Figure 1). The values of n_V $(= 6)$ and k_V $(= 0.3\ \mathrm{d}^{-1})$ were selected so that the time a
163 person spends in $V_1, \ldots, V_{n_V}$, which we will denote as t_V, is distributed approximately the same as
164 $\tilde{t}_V$, the waiting time between vaccination of a previously uninfected person and detection of
165 vaccine-induced SARS-CoV-2-specific IgG antibodies *(4)* (Appendix Figure 8). According to
166 the model, the time that a person spends in $V_1, \ldots, V_{n_V}$ is distributed according to the probability

density function $f(t_V; n_V, k_V) = k_V^{n_V} t_V^{n_V - 1} e^{-k_V t_V} / (n_V - 1)!$, i.e., t_V is Erlang distributed with shape parameter $n_V = 6$ and rate parameter $k_V = 0.3\ \mathrm{d}^{-1}$. As can be seen in Appendix Figure 8, the cumulative distribution function of this Erlang distribution reasonably captures the empirical cumulative distribution of waiting times observed in the longitudinal study of Korodi et al. *(4)*. Thus, in the model, passage through $V_1, \ldots, V_6$ with rate constant $k_V = 0.3\ \mathrm{d}^{-1}$ accounts for the variable and significantly non-zero amount of time required for development of a protective antibody response after vaccination.

The parameters $f_0 > f_1$, $f_1 > f_2$, and f_2 are fractions that characterize the average effectiveness of vaccines used in the US and that determine the sizes of (mutually exclusive) subpopulations of vaccinated persons having different susceptibilities to productive infection (i.e., an infection that can be transmitted to others): $S_{V,1}$, $S_{V,2}$, $S_{V,3}$, and $S_{V,4}$ (Figure 1, Appendix Figure 1). We assume that persons in the $S_{V,1}$ subpopulation are susceptible to productive infection by any of the viral strains considered, and in contrast, we assume that persons in the $S_{V,4}$ subpopulation are susceptible to productive infection by none of the viral strains considered. Persons in the $S_{V,2}$ subpopulation are taken to be susceptible to productive infection by the Alpha and Delta variants but not viral strains in circulation before the emergence of Alpha. Persons in the $S_{V,3}$ subpopulation are taken to be susceptible to productive infection by the Delta variant but not the Alpha variant or viral strains in circulation before the emergence of Alpha. The quantity $1 - f_0$ defines the fraction of vaccinated persons who enter the $S_{V,1}$ subpopulation after exiting V_6, the quantity $f_0 - f_1$ defines the fraction of vaccinated persons who enter the $S_{V,2}$ subpopulation after exiting V_6, the quantity $f_1 - f_2$ defines the fraction of vaccinated persons who enter the $S_{V,3}$ subpopulation after exiting V_6, and f_2 defines the fraction of vaccinated

189 persons who enter the $S_{V,4}$ subpopulation after exiting V_6. We take f_0 to characterize vaccine
190 effectiveness before the emergence of Alpha. According to Thompson et al. *(5)*, vaccine
191 effectiveness was initially 90%. Thus, we set $f_0 = 0.9$. We take f_1 to characterize vaccine
192 effectiveness after the emergence of Alpha but before the emergence of Delta. According to
193 Puranik et al. *(6)*, in May 2021, vaccine effectiveness was 81%. Thus, we set $f_1 = 0.81$. We take
194 f_2 to characterize vaccine effectiveness after the emergence of Delta. According to Tang et al.
195 *(7)*, the effectiveness of two doses of the Pfizer-BioNTech vaccine (BNT162b2) against Delta is
196 53.5% and the effectiveness of two doses of the Moderna vaccine (mRNA-1273) against Delta is
197 84.8%. Taking the average of these figures, we set $f_2 = 0.69$.

198 The parameter m_h characterizes the reduced risk of severe disease for a vaccinated
199 person in the case of a breakthrough infection. We set $m_h = 0.04$, i.e., we assumed that there is a
200 25-fold reduction in the risk of severe disease for infected persons who have been vaccinated,
201 which is consistent with the observations of Lopez Bernal et al. *(8)*.

202 **Notable New Modeling Assumptions**

203 It should be noted that we treat the incubation period for newly infected (exposed)
204 vaccinated persons differently than for newly infected (exposed) unvaccinated persons (Figure 1,
205 Appendix Figure 1). For unvaccinated persons, as in the study of Lin et al. *(1)*, we divide
206 exposed persons in the incubation period of infection into five subpopulations: $E_{1,M}, \dots, E_{5,M}$ for
207 exposed persons who are mixing (i.e., persons who are not practicing social distancing),
208 $E_{1,P}, \dots, E_{5,P}$ for exposed persons who are practicing social distancing, and $E_{1,Q}, \dots, E_{5,Q}$ for
209 exposed quarantined persons. Persons move through the five stages of the incubation period
210 sequentially. In contrast, as a simplification, for vaccinated persons, we consider only a single

exposed population: E_V. We take persons to exit E_V with rate constant $k_L/5$ (Appendix Figure 1). With this choice, the duration of the incubation period of infection is the same, on average, for both vaccinated and unvaccinated persons. The average duration is $5/k_L$ (about 5 d) in both cases. The difference is that the duration of the incubation period is Erlang distributed for unvaccinated persons, as discussed by Lin et al. *(1)*, but exponentially distributed for vaccinated persons.

As indicated in Equation (29), we take vaccinated persons with productive infections to be equally as infectious as unvaccinated persons.

As noted earlier, we take all vaccinated persons to be mixing (i.e., to not be practicing social distancing). Thus, populations of infected vaccinated persons (E_V, I_V, and A_V) contribute to $\phi_M(t)$ (Appendix Equation 29) but not $\phi_P(t)$ (Appendix Equation 30).

As indicated in Appendix Equation 31, we consider pre-symptomatic exposed and asymptomatic unvaccinated persons to be eligible for vaccination and, thus, these persons contribute to the consumption of vaccine doses (i.e., these persons account for a portion of the number of completed vaccinations on a given day i, $\mu_i S_0 \times 1$ d). However, we do not move these persons to vaccinated compartments. The reason is that exposed and asymptomatic persons are expected to develop immunity faster through recovery from infection (i.e., movement to R_U) than from vaccination.

As indicated in Appendix Equation 31, we do not consider symptomatic, quarantined, severely ill and hospitalized/isolated-at-home, or deceased persons to be eligible for vaccination.

Inference and Forecasting Approach

As in the study of Lin et al. *(1)*, for each MSA, we inferred MSA-specific adjustable parameter values θ_F as new MSA-specific surveillance data became available, typically daily. We took a Bayesian inference approach, meaning that, for a given dataset, we generated parameter posterior samples (a collection of θ_F's) through Markov chain Monte Carlo (MCMC) sampling. The parameter posterior samples provide a probabilistic characterization of the adjustable parameter values consistent with the dataset used in inference. By drawing from the parameter posterior samples, we generated a posterior predictive distribution for $I(t_i, t_{i+1})$ for each i (day) of interest. We typically considered all days from January 21, 2020 to the present day and for 14 days into the future. In other words, for each i (day) of interest, a prediction for $I(t_i, t_{i+1})$ was generated for each of many θ_F's drawn randomly (with uniform probability) from the parameter posterior samples. The resulting distribution of $I(t_i, t_{i+1})$ values is the posterior predictive distribution for $I(t_i, t_{i+1})$. Recall that $I(t_i, t_{i+1})$ is given by Appendix Equation 40 and corresponds to $\mathbb{E}[\delta C_i]$, the expected number of new COVID-19 cases detected over a 1-d surveillance interval and reported for the ith day after January 21, 2020. Observation noise was injected into the posterior predictive distributions by replacing each sampled value for $I(t_i, t_{i+1})$ with $X_i \sim \mathrm{NB}(r, q_i)$, where r is a member of the sampled set of parameter values θ_F used to generate the prediction of $I(t_i, t_{i+1})$ and q_i is given by Equation 43.

According to Bayes' theorem, given surveillance data $D = \{\delta C_i\}_{i=0}^{d}$, the parameter posterior is

$$\mathbb{P}\{\theta_F | D\} = \frac{\mathbb{P}\{D | \theta_F\}\, \mathbb{P}\{\theta_F\}}{Z} \tag{44}$$

where $\mathbb{P}\{\theta_F\}$ is the prior (which is formulated to capture knowledge of θ_F external to D or to express lack of such knowledge), $\mathbb{P}\{D | \theta_F\}$ is the likelihood defined by Appendix Equations 41–

43, and Z is a normalizing constant. We assumed a proper uniform prior, i.e., for each adjustable parameter, we assumed that all values between specified lower and upper bounds are equally likely before consideration of D. We used the same bounds as in the study of Lin et al. *(1)*. Then we used an adaptive MCMC (aMCMC) algorithm *(9)* to generate samples of $\mathbb{P}\{D|\theta_F\}\,\mathbb{P}\{\theta_F\}$, which is proportional to $\mathbb{P}\{\theta_F|D\}$. Thus, the relative probabilities of parameter sets θ_F according to $\mathbb{P}\{\theta_F|D\}$ are correctly represented by the samples.

We used an adaptive MCMC algorithm *(9)* to generate samples of the multivariate parameter posterior for adjustable model parameters (t_0, β, and parameters for variant emergence and social distancing), the measurement model parameter f_D, and the likelihood parameter r (Table 1). The aMCMC algorithm is available within the PyBioNetFit software package. Use of the algorithm was as described by Lin *et al. (1).* The report of Neumann et al. *(10)* includes helpful general usage advice, which was followed in this study. Daily inference jobs were executed on a computer cluster.

Each inference was conditioned on the compartmental model of Figure 1 (Appendix Equations 1–38), settings for the structural parameters m (the number of SARS-CoV-2 variants under consideration) and n (the number of social-distancing periods under consideration beyond an initial social-distancing period), the measurement model (Appendix Equations 39 and 40), and fixed parameter estimates (Table 2), including empirical daily *per capita* vaccination rates (i.e., the settings for μ_i in Appendix Equation 37). We assumed a proper uniform prior for each adjustable parameter *(1)* and a negative binomial likelihood function (Appendix Equations 41–43). Use of a uniform prior means that MAP estimates are maximum likelihood estimates (MLEs). In each inference, the data entering the likelihood function, $D = \{\delta C_i\}_{i=0}^{d}$ (Appendix

Equation 41), were MSA-specific daily reports of newly detected COVID-19 cases available up to the date of inference $\mathcal{D}_{\mathrm{d}}$ (i.e., the dth day after January 21, 2020). Thus, all inferences are region-specific and time-dependent. We made inferences daily as new surveillance and vaccination data became available.

Use of Model Selection to Determine Intervals of Step Functions

Variant takeover times, $\theta = (\theta_1, \theta_2)$, and start times of social-distancing periods, $\tau = (\tau_1, \dots, \tau_n)$, were inferred from data; however, changes of the associated time-dependent step functions, $Y_\theta(t)$, $P_\tau(t)$, and $\Lambda_\tau(t)$, were introduced only when an increase in model complexity was deemed to be justified. Each decision to introduce variant takeover or start of a new social-distancing period (beyond the initial period) was made using a model-selection procedure, which is described below. It should be noted that y_1 and y_2 are parameters of $Y_\theta(t)$, $p_0, p_1, \dots, p_n$ are parameters of $P_\tau(t)$, and $\lambda_0, \lambda_1, \dots, \lambda_n$ are parameters of $\Lambda_\tau(t)$. These parameters determine the values of the step functions over different periods. For example, for $n \geq 1$, p_1 is the value of $P_\tau(t)$ and λ_1 is the value of $\Lambda_\tau(t)$ for the period $t \in [\tau_1, \tau_2)$. Similarly, y_1 is the value of $Y_\theta(t)$ for the period $t \in [\theta_1, \theta_2)$, and y_2 is the value of $Y_\theta(t)$ for the period $t \in [\theta_2, \infty)$ (or until a new variant supplants Delta as the dominant circulating viral strain).

The start times of social-distancing periods were determined using the model-selection procedure previously described *(1)*. This procedure involves calculating values for the Akaike information criterion (AIC) and the Bayesian information criterion (BIC) *(11)* for two versions of the model with different settings for n, namely, versions with $n := \hat{n}$ and $n := \hat{n} + 1$, where $\hat{n}$ is the current number of social-distancing periods beyond the initial social-distancing period. Thus, the version of the model with the setting $n := \hat{n}$ is the version considered to provide the

best (most parsimonious) explanation of all currently available surveillance data. Initially, when online learning begins, $\hat{n} := 0$. On a given inference day d, we perform multiple inferences, considering different values for n (and also m), and in each inference, we find $\hat{\mathcal{L}}_{n,m} = \max_{\theta_F} \mathcal{L}\left(\theta_F(n,m); \{\delta C_i\}_{i=0}^{d}\right)$, where the likelihood $\mathcal{L}$ is defined by Appendix Equations 41–43. We calculate AIC as $2|\theta_F| - 2\ln \hat{\mathcal{L}}_{n,m}$ and BIC as $|\theta_F| \ln d - 2\ln \hat{\mathcal{L}}_{n,m}$, where $|\theta_F|$ is the number of adjustable parameters (i.e., the dimension of θ_F). In a strength-of-evidence comparison, we calculate ΔAIC as $\mathrm{AIC}^{n:=\hat{n}} - \mathrm{AIC}^{n:=\hat{n}+1}$ and ΔBIC as $\mathrm{BIC}^{n:=\hat{n}} - \mathrm{BIC}^{n:=\hat{n}+1}$, where $\mathrm{AIC}^{n:=\hat{n}}$ ($\mathrm{AIC}^{n:=\hat{n}+1}$) is the AIC value calculated for the $n := \hat{n}$ ($n := \hat{n} + 1$) version of the model and, similarly, $\mathrm{BIC}^{n:=\hat{n}}$ ($\mathrm{BIC}^{n:=\hat{n}+1}$) is the BIC value calculated for the $n := \hat{n}$ ($n := \hat{n} + 1$) version of the model. We increment $\hat{n}$ (i.e., we perform the update $\hat{n} \leftarrow \hat{n} + 1$) whenever $\Delta\mathrm{AIC}>10$ and $\Delta\mathrm{BIC}>10$.

In the extended model, the value of the step function $Y_\theta(t)$ characterizes disease transmissibility in a given region at time t relative to that in 2020. The value of $Y_\theta(t)$ increases when a new strain (Alpha or Delta) becomes the dominant circulating strain. Alpha was taken to supplant ancestral strains at time $t = \theta_1$ in 2021, and Delta was taken to supplant Alpha at a time $t = \theta_2 > \theta_1$. The Alpha takeover time θ_1 was determined using a model selection procedure similar to that used to determine start times of new social-distancing periods *(1)*. Starting in 2021, we considered two versions of the model, denoted as M1 and M2. In M1, $Y_\theta(t)$ has a single value (of 1) over the entire period of concern (from January 21, 2020 to the current date). In M2, there are two distinct values (namely, 1 and y_1), with the second value replacing the first at time $t = \theta_1$ (which is constrained to fall after December 31, 2020). In M2, the setting for θ_1 was inferred jointly with other region-specific model parameter values. To determine whether to

admit Alpha takeover, we calculated $\Delta\text{AIC} \equiv \text{AIC}^{\text{M1}} - \text{AIC}^{\text{M2}}$ and $\Delta\text{BIC} \equiv \text{BIC}^{\text{M1}} - \text{BIC}^{\text{M2}}$ and selected M2 (i.e., we admitted Alpha takeover) whenever $\Delta\text{AIC} > 10$ and $\Delta\text{BIC} > 10$. At times beyond $t = \theta_1$, the Delta takeover time θ_2 was determined through essentially the same approach, except that we considered versions of the model with either two or three different $Y_\theta(t)$ values. In other words, we decided between model versions M2 and M3, where in M3, there are three distinct $Y_\theta(t)$ values (namely, 1, y_1, and y_2) with the third value replacing the second at time $t = \theta_2$.

Simulations

After specification of parameter values (Tables 1 and 2), we used the SciPy (https://www.scipy.org) interface to LSODA *(12)* to numerically integrate the system of coupled ODEs consisting of the 40 ODEs of the compartmental model and the 1 ODE of the measurement model (Appendix Equations 1–39). The initial condition was defined by settings for t_0, I_0, and S_0 (Tables 1 and 2). Integration combined with use of Appendix Equation 40 yielded a prediction of the expected number of new cases detected for each 1-d surveillance period of interest in the past or future: $I(t_i, t_{i+1})$, where t_i corresponds to midnight on the ith day after January 21, 2020. To account for randomness in case detection and reporting, we replaced $I(t_i, t_{i+1})$ with $X_i \sim \text{NB}(r, q_i)$, where q_i is given by Appendix Equation 43.

Method for Assessing Forecast Accuracy

We used out-of-sample data to assess forecast accuracy. We calculated coverage for each of the following 21 prediction quantiles: $0.025, 0.05, 0.1, 0.15, 0.2, \ldots, 0.9, 0.95, 0.975$. We considered four prediction horizons: 1-, 4-, 7-, and 14-d ahead. For purposes of illustration, let us focus on the 7-d ahead prediction horizon and the 90th prediction quantile (corresponding to the

90th percentile of the posterior predictive distribution for number of new cases detected on a given day). On day T, for each of the 15 MSAs of interest, using all MSA-specific data available before $t = T$ (the in-sample data), we generated a posterior predictive distribution for $t = T + 1\text{ d}, T + 2\text{ d}, \cdots, T + 14\text{ d}$. For each MSA, from the posterior predictive distribution for $t = T + 7\text{ d}$, we obtained a 90th percentile prediction of the number of new cases detected over a 1-d period for $t = T + 7\text{ d}$. model. Let us use $I_M^{90}(T + 7\text{ d})$ to denote the 90th percentile prediction of number of cases detected at the 7-d ahead prediction horizon for the Mth MSA. Note that 90% of predictions making up the posterior predictive distribution fall at or below $I_M^{90}(T + 7\text{ d})$. Let us use $\delta C_{T+7\text{ d},M}$ to denote the actual number of cases detected at the 7-d ahead prediction horizon (the out-of-sample data) for the Mth MSA. We considered all daily forecasts made from July 15, 2021 to August 24, 2021. The coverage corresponding to the 7-d ahead prediction horizon and the 90th prediction quantile was calculated as the fraction of times that $C_{T+7\text{ d},M}$ was less than or equal to $I_M^{90}(T + 7\text{ d})$. Missing daily case reports were imputed as described previously.

Appendix References

1. Lin YT, Neumann J, Miller EF, Posner RG, Mallela A, Safta C, Ray J, Thakur G, Chinthavali S, Hlavacek WS. Daily forecasting of regional epidemics of Coronavirus Disease with Bayesian uncertainty quantification, United States. Emerg Inf Dis. 2021;27:767–78. https://doi.org/10.3201/eid2703.203364
2. Executive Office of the President. OMB bulletin no. 15-01. 2020 [cited 2021 Oct 8]. https://www.bls.gov/bls/omb-bulletin-15-01-revised-delineations-of-metropolitan-statistical-areas.pdf

363 3. Covid Act Now. US COVID risk and vaccine tracker. 2021 [cited 2021 Sep 29]
364 https://covidactnow.org/
365 4. Korodi M, Rákosi K, Jenei Z, Hudák G, Horváth I, Kákes M, et al. Longitudinal
366 determination of mRNA-vaccination induced strongly binding SARS-CoV-2 IgG
367 antibodies in a cohort of healthcare workers with and without prior exposure to the novel
368 coronavirus. https://www.medrxiv.org/content/10.1101/2021.03.17.21253751v1
369 5. Thompson MG, Burgess JL, Naleway AL, Tyner HL, Yoon SK, Meece J, et al. Interim
370 estimates of vaccine effectiveness of BNT162b2 and mRNA-1273 COVID-19 vaccines
371 in preventing SARS-CoV-2 infection among health care personnel, first responders, and
372 other essential and frontline workers—eight U.S. locations, December 2020–March 2021.
373 MMWR Morb Mortal Wkly Rep. 2021;70:495–500.
374 http://dx.doi.org/10.15585/mmwr.mm7013e3
375 6. Puranik A, Lenehan PJ, Silver E, Niesen MJM, Corchado-Garcia J, O'Horo JC, et al.
376 Comparison of two highly-effective mRNA vaccines for COVID-19 during periods of
377 Alpha and Delta variant prevalence. [cited 2021 Oct 8]
378 https://www.medrxiv.org/content/10.1101/2021.08.06.21261707v3
379 7. Tang P, Hasan MR, Chemaitelly H, Yassine HM, Benslimane FM, Al Khatib HA, et al.
380 BNT162b2 and mRNA-1273 COVID-19 vaccine effectiveness against the Delta
381 (B.1.617.2) variant in Qatar. [cited 2021 Oct 8]
382 https://www.medrxiv.org/content/10.1101/2021.08.11.21261885v1
383 8. Lopez Bernal J, Andrews N, Gower C, Gallagher E, Simmons R, Thelwall S, et al.
384 Effectiveness of Covid-19 Vaccines against the B.1.617.2 (Delta) variant. N Engl J Med.
385 2021;385:585–94. https://doi.org/10.1056/NEJMoa2108891

9. Andrieu C, Thoms J. A tutorial on adaptive MCMC. Stat Comput. 2008;18:343–73.
10. Neumann J, Lin YT, Mallela A, Miller EF, Colvin J, Duprat AT, Chen Y, Hlavacek WS, Posner RG. Implementation of a practical Markov chain Monte Carlo sampling algorithm in PyBioNetFit. https://arxiv.org/abs/2109.14445
11. Burnham KP, Anderson DR. Multimodal inference: understanding AIC and BIC in model selection. Sociol Methods Res. 2004;33:261–304. https://doi.org/10.1177/0049124104268644
12. Hindmarsh AC. ODEPACK, a systematized collection of ODE solvers. In Stepleman RS, editor. Scientific computing: applications of mathematics and computing to the physical sciences. Amsterdam: North-Holland Publishing Company; 1983. p. 55–64.

397

Appendix Table 1. State variables of the compartmental model

State variable (population)	Description
S_M	Population of susceptible unvaccinated persons who are mixing (i.e., not practicing social distancing)
S_P	Population of susceptible unvaccinated persons who are practicing social distancing
$S_{V,1}$	Population of vaccinated unexposed persons who developed an immune response to vaccination that does not protect against productive infection by ancestral strains or the Alpha and Delta variants
$S_{V,2}$	Population of vaccinated unexposed persons who developed an immune response to vaccination that protects against productive infection by ancestral strains but not the Alpha or Delta variants
$S_{V,3}$	Population of vaccinated unexposed persons who developed an immune response to vaccination that protects against productive infection by ancestral strains and the Alpha variant but not the Delta variant
$S_{V,4}$	Population of vaccinated unexposed persons who developed an immune response to vaccination that protects against productive infection by ancestral strains and the Alpha and Delta variants
V_i $(i = 1, \dots, 6)$	Population of vaccinated persons in the ith stage of immune response to vaccination
$E_{i,M}$ $(i = 1, \dots, 5)$	Population of exposed unvaccinated persons in the ith stage of the incubation period of infection and who are mixing
$E_{i,P}$ $(i = 1, \dots, 5)$	Population of exposed unvaccinated persons in the ith stage of the incubation period of infection and who are practicing social distancing
$E_{i,Q}$ $(i = 2, \dots, 5)$	Population of exposed unvaccinated persons in the ith stage of the incubation period of infection and who are quarantined
E_V	Population of vaccinated persons in the incubation period of a productive infection (i.e., an infection that can be transmitted to others)

A_M	Population of asymptomatic unvaccinated persons who are in the immune clearance phase of infection and who are mixing
A_P	Population of asymptomatic unvaccinated persons who are in the immune clearance phase of infection and who are practicing social distancing
A_Q	Population of asymptomatic unvaccinated persons who are in the immune clearance phase of infection and who are quarantined
A_V	Population of asymptomatic vaccinated persons who are in the immune clearance phase of a productive infection (i.e., an infection that can be transmitted to others)
I_M	Population of infectious, symptomatic, and unvaccinated persons with mild disease who are mixing
I_P	Population of infectious, symptomatic, non-vaccinated, and infectious persons with mild disease who are practicing social distancing
I_Q	Population of infectious, symptomatic, and unvaccinated persons with mild disease who are quarantined
I_V	Population of infectious, symptomatic, and vaccinated persons with mild disease
R_U	Population of recovered unvaccinated persons
R_V	Population of recovered vaccinated persons
H_U	Population of unvaccinated persons with severe disease who are hospitalized or isolated at home
H_V	Population of vaccinated persons with severe disease who are hospitalized or isolated at home
D	Population of deceased persons

398

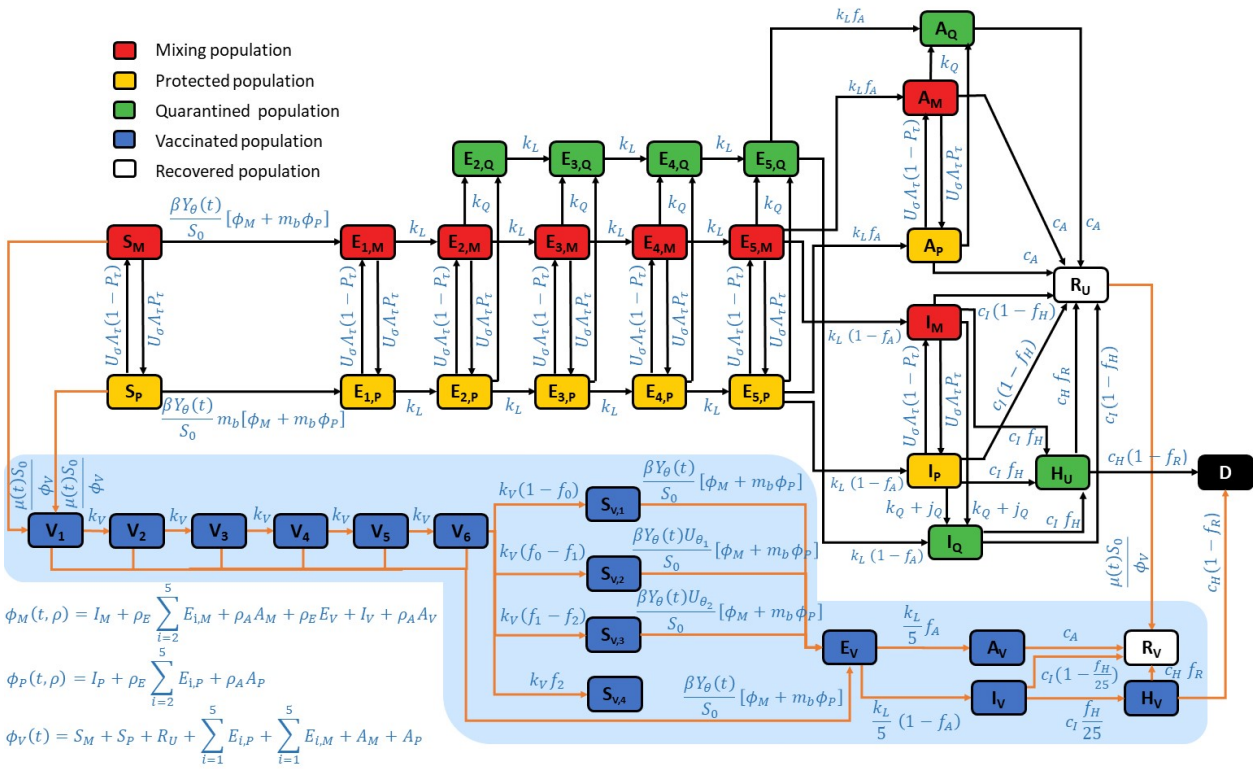

Appendix Figure 1. Expanded illustration of the new compartmental model. In the extended model, vaccination was considered by allowing susceptible and recovered persons to transition into a vaccinated compartment, either V_1 and R_V. Susceptible (recovered) persons who have completed vaccination move into the V_1 (R_V) compartment. The susceptible persons who move into V_1 are drawn from S_M (populated by susceptible persons who are mixing and unprotected by social distancing) and from S_P (populated by susceptible persons who are protected by social distancing). After susceptible persons enter V_1, they can move through a series of additional compartments (V_2 through V_6), which are included to capture the time needed for immunity to develop after completion of vaccination. We estimate that the time needed to acquire immunity after vaccination is approximately three weeks based on longitudinal studies of anti-spike protein IgG levels *(4)*. Persons who exit the V_6 compartment without becoming infected enter one of the following compartments: $S_{V,1}$, $S_{V,2}$, $S_{V,3}$, or $S_{V,4}$. Persons in $S_{V,1}$ are taken to remain susceptible

412 to productive infection by all SARS-CoV-2 strains of interest (Alpha, Delta, and ancestral
413 strains). Persons in $S_{V,2}$ are taken to be susceptible to SARS-CoV-2 Alpha and Delta variants.
414 Persons in $S_{V,3}$ are taken to be susceptible to Delta. Persons in $S_{V,4}$ are taken to be protected
415 against all strains of interest. Infection of persons in $S_{V,3}$ is only allowed if Delta is present, i.e.,
416 at times $t > \theta_2$. Infection of persons in $S_{V,2}$ is only allowed if Alpha or Delta is present, i.e., at
417 times $t > \theta_1$. Vaccinated persons in compartments V_1 through V_6 and compartment $S_{V,1}$ are
418 allowed to become infected at any time, at which point they transition to compartment E_V,
419 consisting of vaccinated persons who were exposed before development of vaccine-induced
420 immunity. Persons in compartment $S_{V,2}$ are allowed to become infected if $t \geq \theta_1$. Similarly,
421 persons in compartment $S_{V,3}$ are allowed to become infected if $t \geq \theta_2$. Possible outcomes for
422 persons in E_V are taken to be the same as those for unvaccinated exposed persons; however, the
423 incubation period is taken to be distinct. Persons in E_V can experience asymptomatic disease
424 (upon entering A_V) or they can become symptomatic (upon entering I_V). Persons in A_V
425 eventually recover, entering compartment R_V. Persons in I_V can progress to severe disease (upon
426 entering H_V) or recover (upon entering R_V). Persons in H_V either recover (moving into R_V) or die
427 (moving into D). Persons who have recovered from infection, in the R_U compartment, move
428 directly into the R_V compartment upon vaccination. Persons in the R_U and R_V compartments are
429 taken to have full immunity. The vaccination rate at which susceptible and recovered persons
430 move into vaccinated compartments is updated daily for consistency with the empirical overall
431 rate of vaccination, which we extract daily from COVID Act Now Data API *(3)*. The relative
432 values of the vaccination rate are set such that each person eligible for vaccination has the same
433 probability of being vaccinated. All unvaccinated persons are taken to be eligible for vaccination
434 except symptomatic persons (in compartments I_M and I_P), persons who are hospitalized or

severely ill at home (in compartment H), quarantined persons (in the various compartments labeled with a Q subscript), and deceased persons (in compartment D). It should be noted that asymptomatic, non-quarantined persons (in compartments A_M and A_P) and presymptomatic, non-quarantined persons (in the E compartments) are taken to be eligible (and to influence the vaccination rate constants) but, as a simplification, these persons are not explicitly tracked as vaccinated or unvaccinated because each of these persons will eventually enter either the D compartment or the R_U compartment, at which point they will have immunity. In the model, the effects of SARS-CoV-2 variants are captured by a time-dependent dimensionless multiplier $Y_\theta(t)$ of the rate constant β. This rate constant, which appears in Appendix Equations 1–4, 18–22, and 24, determines the rate of disease transmission within the subpopulation unprotected by social-distancing behaviors when $Y_\theta(t) = 1$. We take $Y_\theta(t) = 1$ for times $t < \theta_1$, i.e., for the initial period of the COVID-19 pandemic in the US that we take to have started on January 21, 2020. We take $Y_\theta(t)$ to have the form of a step function with distinct values greater than 1 for periods starting at $t = \theta_1$ and $\theta_{k+1} > \theta_k$ for $k = 1, \ldots, m$. Thus, the model allows for m distinct periods of variant strain dominance delimited by a set of start times $\theta = \{\theta_1, \ldots, \theta_m\}$. We considered $m = 2$. We constrained θ_1 to fall within 2021. We assume that variants differ only in transmissibility. We introduce new periods of variant strain dominance (i.e., new values for $Y_\theta(t)$) using a model selection procedure, which is the same as that used to introduce new social-distancing periods.

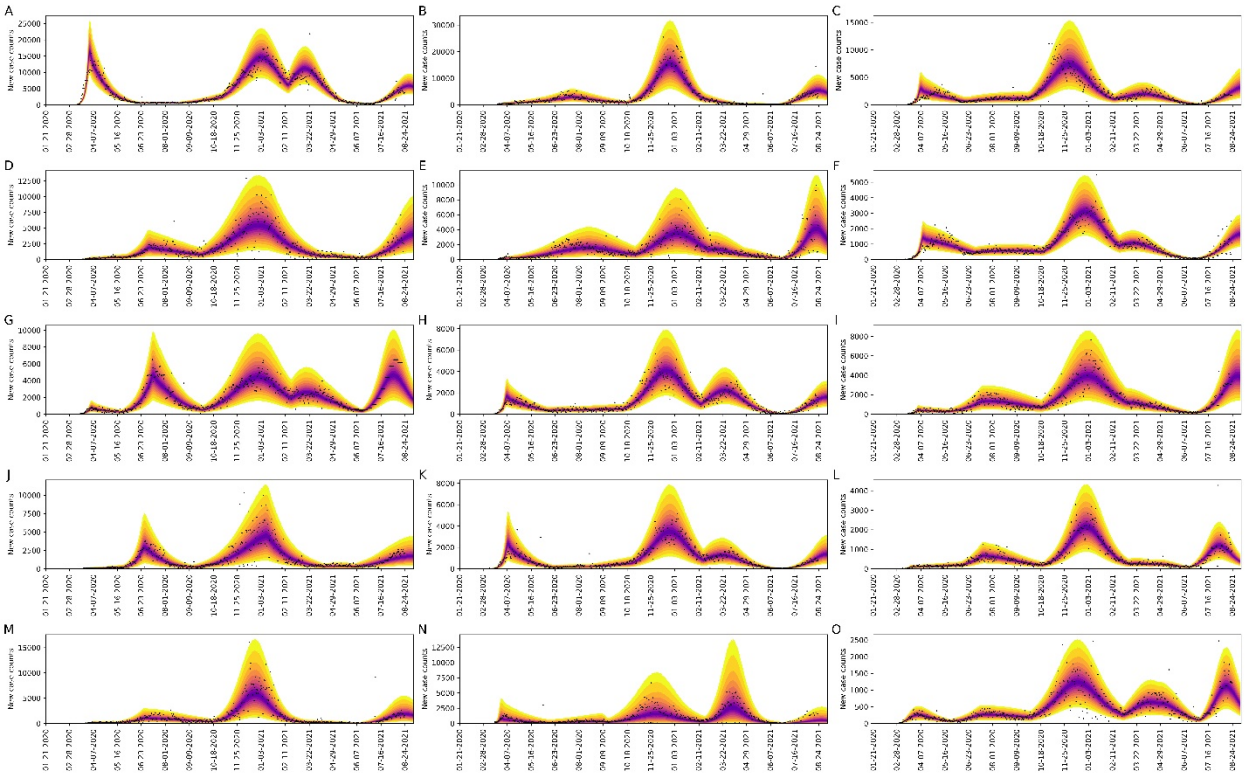

Appendix Figure 2. Posterior predictive checking. This figure is an extension of Figure 2, Panel A for all 15 MSAs of interest: A) New York City, NY; B) Los Angeles, CA; C) Chicago, IL; D) Dallas, TX; E) Houston, TX; F) Washington, DC; G) Miami, FL; H) Philadelphia, PA; I) Atlanta, GA; J) Phoenix, AZ; K) Boston, MA; L) San Francisco, CA; M) Riverside, CA; N) Detroit, MI; and O) Seattle, WA. Each MSA-specific compartmental model was parametrized using the reported daily case numbers available from January 21, 2020 to August 24, 2021 (represented by black crosses in each panel). The shaded region in each panel indicates the 95% credible interval obtained for each indicated posterior predictive distribution for number of daily cases detected and reported. Colors indicate various credible intervals, as indicated in the legend of Figure 2B. Each panel includes a 14-d ahead forecast. The last prediction date was September 7, 2021.

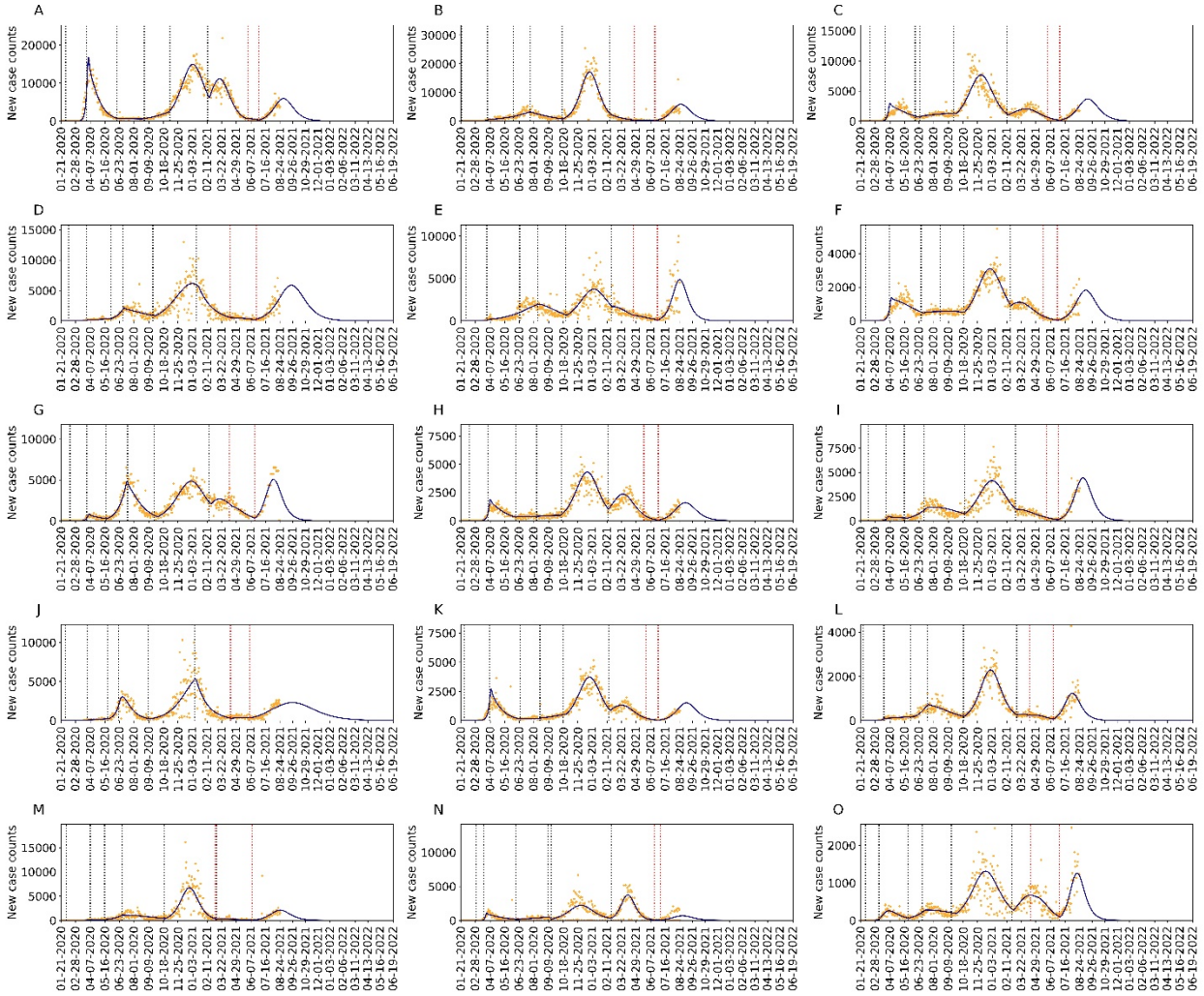

Appendix Figure 3. MLE predictions. This figure is an extension of Figure 2, Panel C for all 15 MSAs of interest: A) New York City, NY; B) Los Angeles, CA; C) Chicago, IL; D) Dallas, TX; E) Houston, TX; F) Washington, DC; G) Miami, FL; H) Philadelphia, PA; I) Atlanta, GA; J) Phoenix, AZ; K) Boston, MA; L) San Francisco, CA; M) Riverside, CA; N) Detroit, MI; and O) Seattle, WA. MSA-specific MAP estimates for adjustable parameters (from inferences described in Appendix Figure 2) were used to extend the curve for number of new cases detected and reported 300-d into the future. The black vertical lines indicate the dates on which social-

distancing parameters changed in the model. The leftmost red vertical line indicates the Alpha takeover time, and the rightmost red vertical line indicates the Delta takeover time.

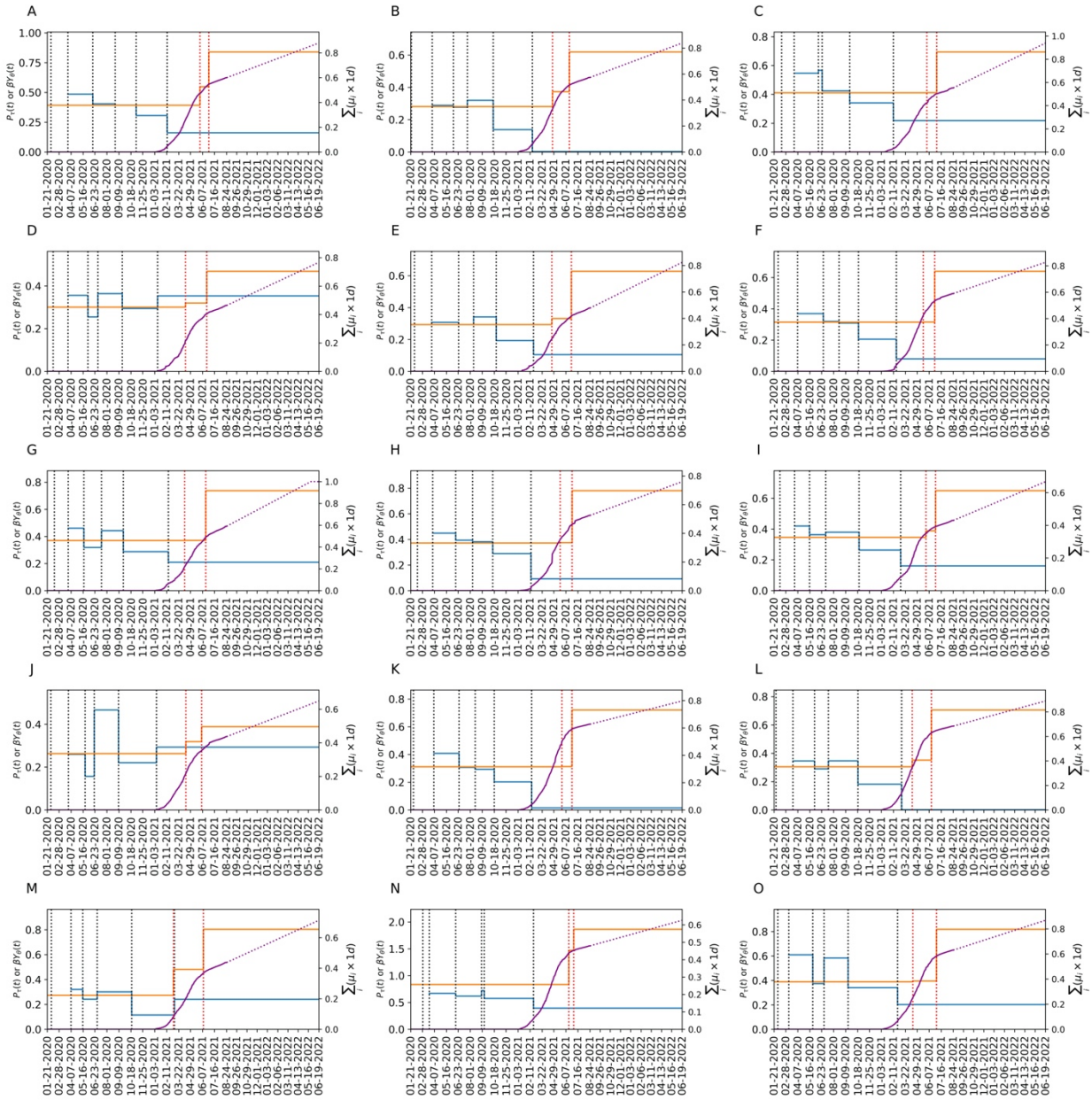

Appendix Figure 4. P_τ and $Y_\theta\beta$ vs. time t (left vertical axis) and $\sum_i(\mu_i \times 1\text{ d})$ vs. time t (right vertical axis). This figure is an extension of Figure 2, Panel D for all 15 MSAs of interest: A) New York City, NY; B) Los Angeles, CA; C) Chicago, IL; D) Dallas, TX; E) Houston, TX; F) Washington, DC; G) Miami, FL; H) Philadelphia, PA; I) Atlanta, GA; J) Phoenix, AZ; K) Boston, MA; L) San Francisco, CA; M) Riverside, CA; N) Detroit, MI; and O) Seattle, WA.

MSA-specific MAP estimates for the setpoint parameter of $P_\tau(t)$ and the transmissibility factor of $Y_\theta(t)$ times β are indicated on the left vertical axis. The actual or projected value of the sum $\sum_i(\mu_i \times 1\text{ d})$ (with each μ_i set using vaccination data as explained in the text of the Appendix) is indicated on the right vertical axis. Parameter estimates are based on the inferences described in Appendix Figure 2.

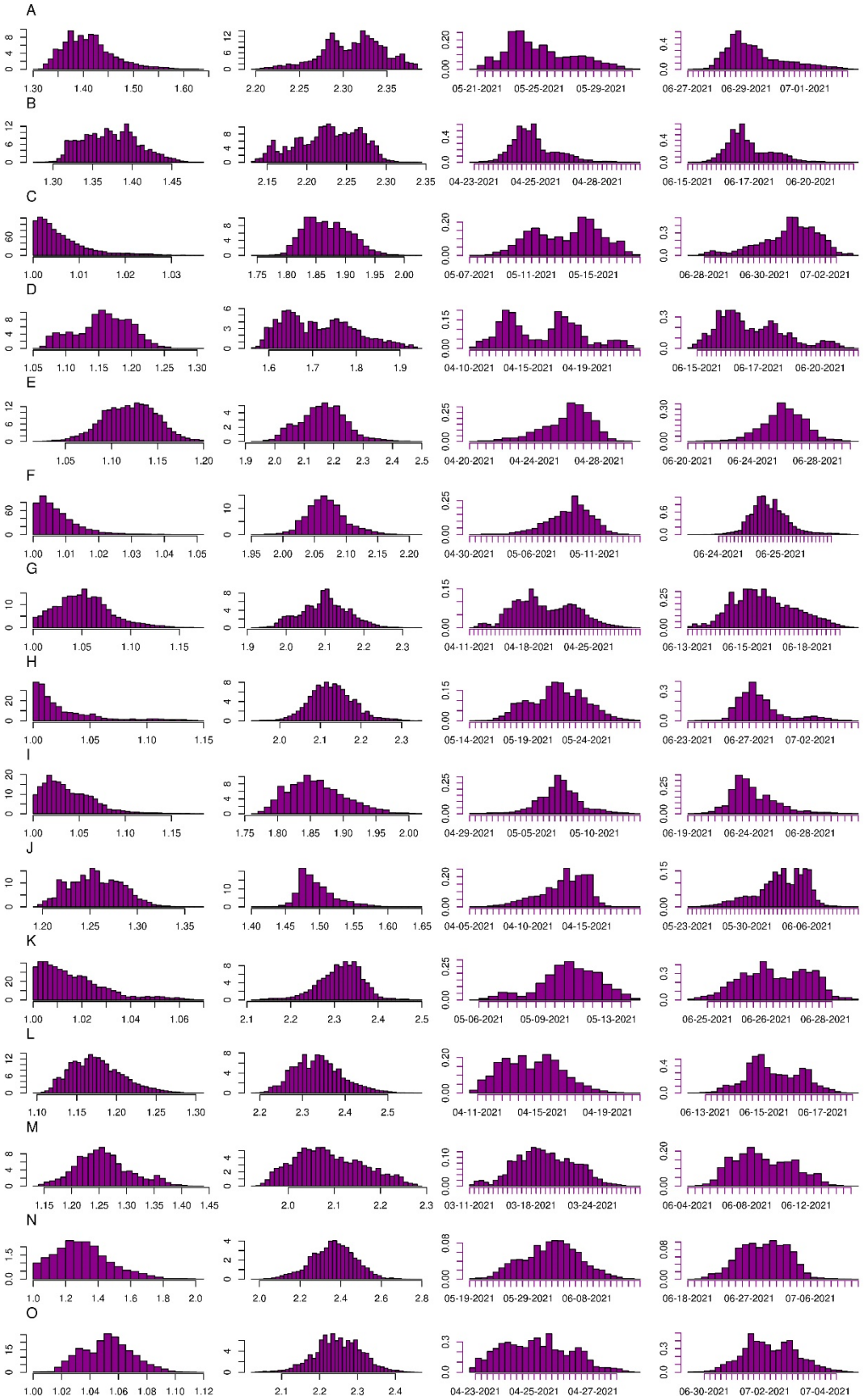

493

Appendix Figure 5. Marginal posteriors for y_1, y_2, θ_1, and θ_2. This figure is an extension of Figure 4 for all 15 MSAs of interest: A) New York City, NY; B) Los Angeles, CA; C) Chicago, IL; D) Dallas, TX; E) Houston, TX; F) Washington, DC; G) Miami, FL; H) Philadelphia, PA; I) Atlanta, GA; J) Phoenix, AZ; K) Boston, MA; L) San Francisco, CA; M) Riverside, CA; N) Detroit, MI; and O) Seattle, WA. Marginal posteriors are shown as histograms and are derived from region-specific parameter posterior samples obtained using surveillance data available from January 21, 2020 to August 24, 2021.

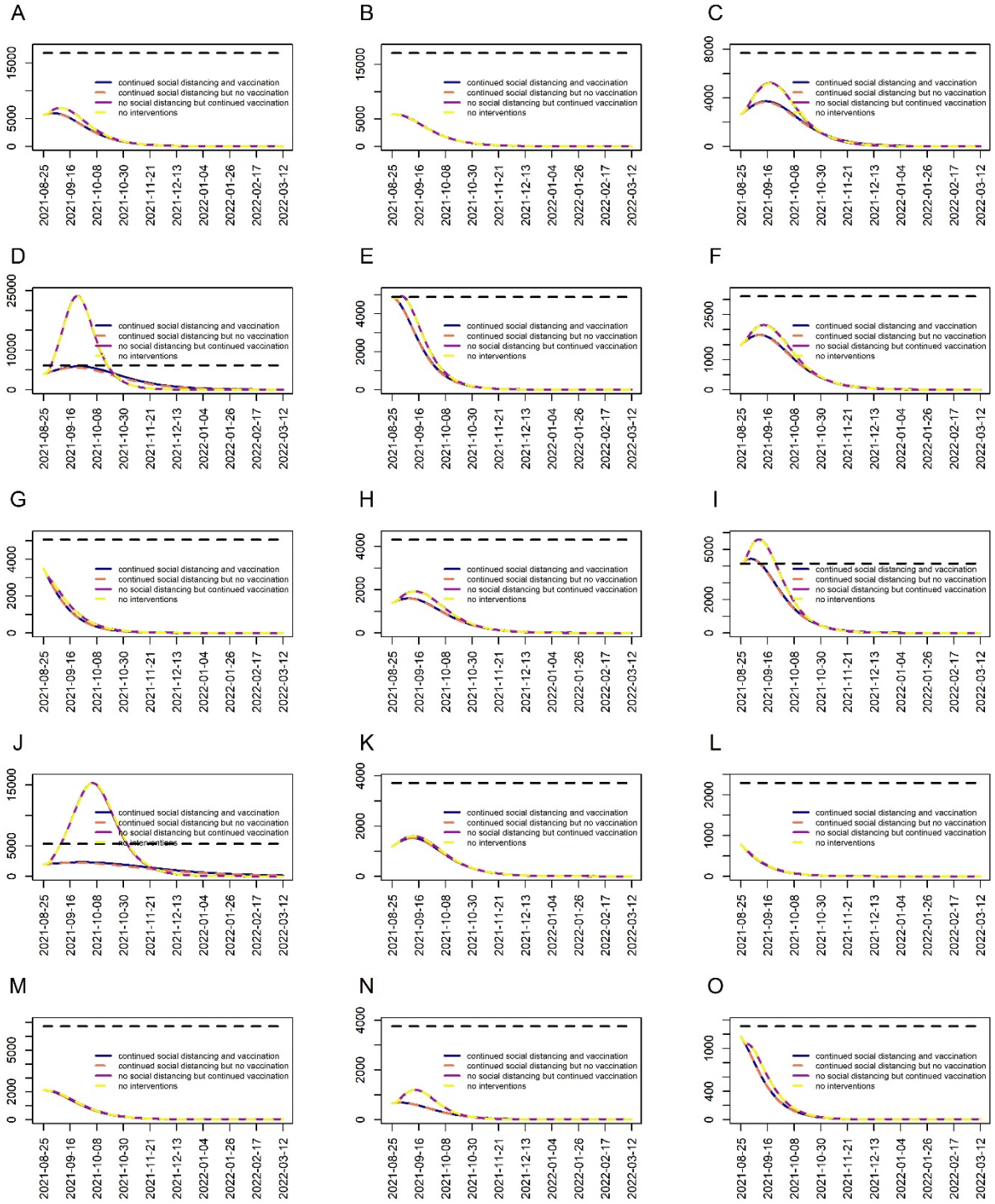

Appendix Figure 6. Projected daily detection of new COVID-19 cases in the face of Delta over a 300-d period (August 24, 2021 to March 12, 2022). This figure is an extension of Figure 6 for 15 MSAs of interest: A) New York City, NY; B) Los Angeles, CA; C) Chicago, IL; D) Dallas,

TX; E) Houston, TX; F) Washington, DC; G) Miami, FL; H) Philadelphia, PA; I) Atlanta, GA; J) Phoenix, AZ; K) Boston, MA; L) San Francisco, CA; M) Riverside, CA; N) Detroit, MI; and O) Seattle, WA. Four projections are made for each MSA, continued social distancing as on August 24, 2021 and vaccination at a daily rate equal to the average empirical daily rate over the 20-d period starting on August 5, 2021 and ending on August 24, 2021 (blue curve), continued social distancing but no vaccination (orange dashed curve), no social distancing but continued vaccination (purple curve) and no interventions (yellow dashed curve). The black horizontal dashed line marks the highest number of new cases detected over any 1-d period.

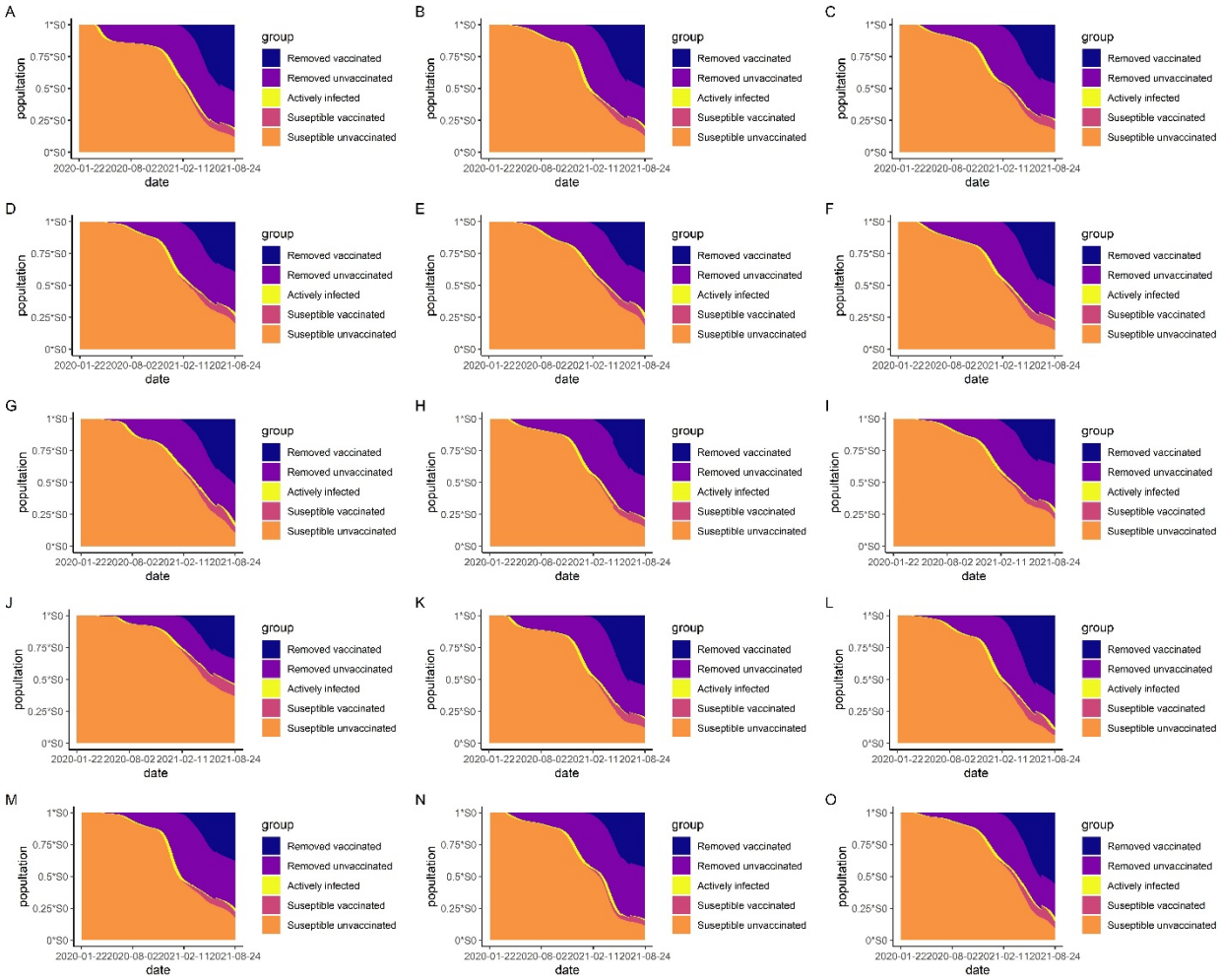

Appendix Figure 7. Subpopulation dynamics. This figure is an extension of Figure 7 for all 15 MSAs of interest: A) New York City, NY; B) Los Angeles, CA; C) Chicago, IL; D) Dallas, TX; E) Houston, TX; F) Washington, DC; G) Miami, FL; H) Philadelphia, PA; I) Atlanta, GA; J) Phoenix, AZ; K) Boston, MA; L) San Francisco, CA; M) Riverside, CA; N) Detroit, MI; and O) Seattle, WA. In each panel, a legend indicates the subpopulations considered, and the subpopulation dynamics shown are based on MAP estimates from inferences using region-specific surveillance data available from January 21, 2020 to August 24, 2021.

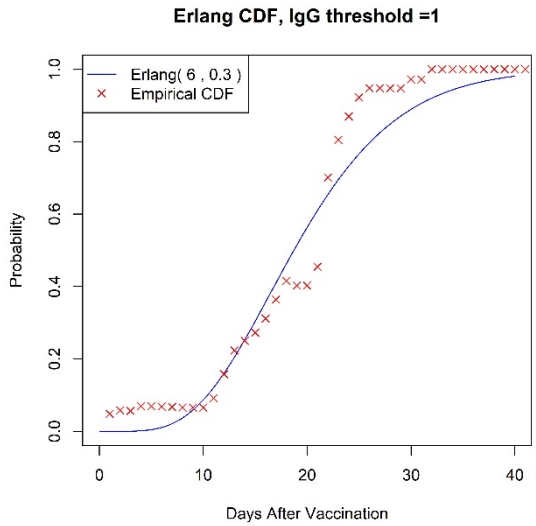

Appendix Figure 8. Comparison of an Erlang cumulative distribution function with shape parameter $n_V = 6$ and rate parameter $k_V = 0.3\ \mathrm{d}^{-1}$ and the empirical cumulative distribution of waiting times ($\tilde{t}_V$ values) observed in the longitudinal study of Korodi et al. *(4)*. The waiting time $\tilde{t}_V$ is the time between vaccination of a previously uninfected person and detection of vaccine-induced SARS-CoV-2-specific IgG antibodies.